Supporting Information

Cyclometalated Ru(II) complexes with tunable redox and optical properties for dye-sensitized solar cells

Maria A. Lavrova, Sergey A. Mishurinskiy, Daniil E. Smirnov, Paulina Kalle, Ekaterina V. Krivogina, Sergey A. Kozyukhin, Viktor V. Emets, Sofia S. Mariasina, Vladimir D. Dolzhenko, and Stanislav I. Bezzubov*

Table of Content

1. **NMR and mass spectra**

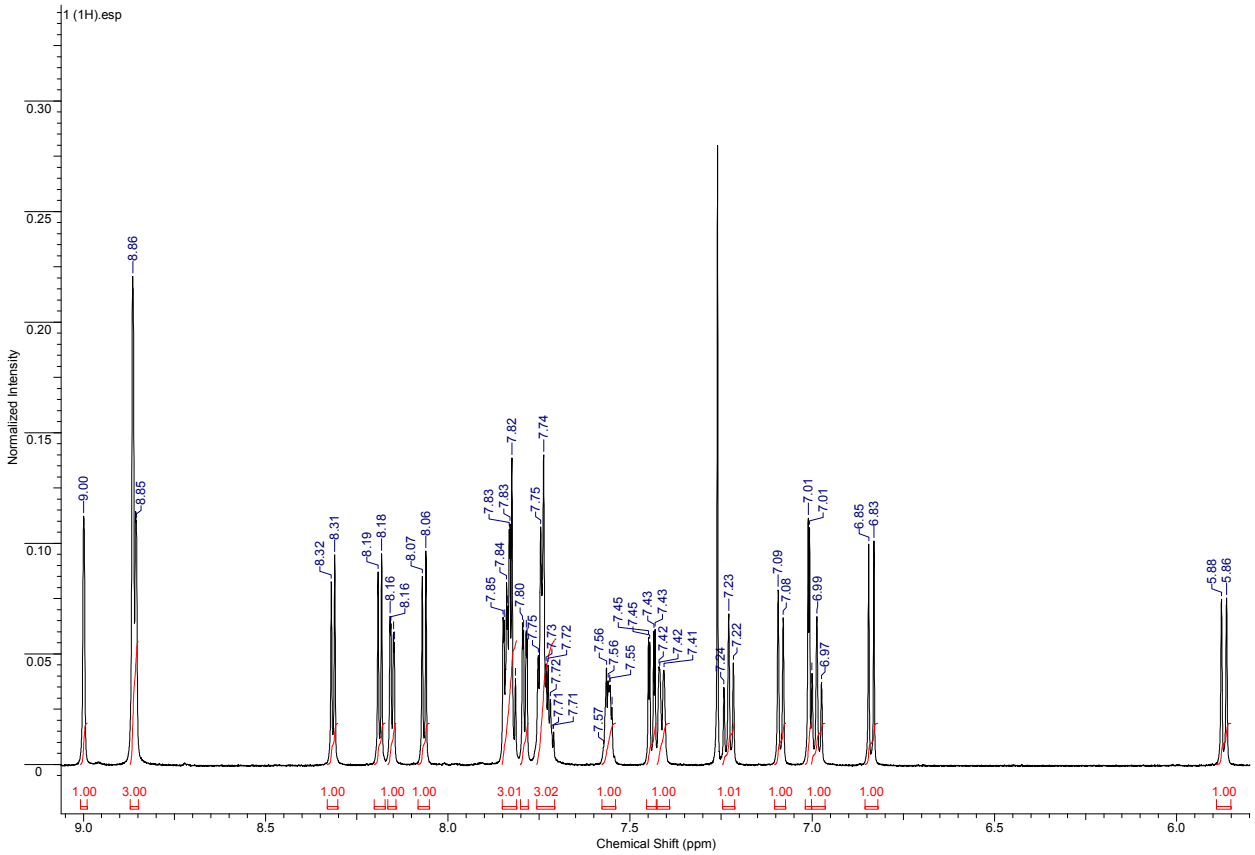

Figure S1. Aromatic region of ^{1}H NMR spectrum of **1** (600 MHz, 298K, $CDCl_3$).

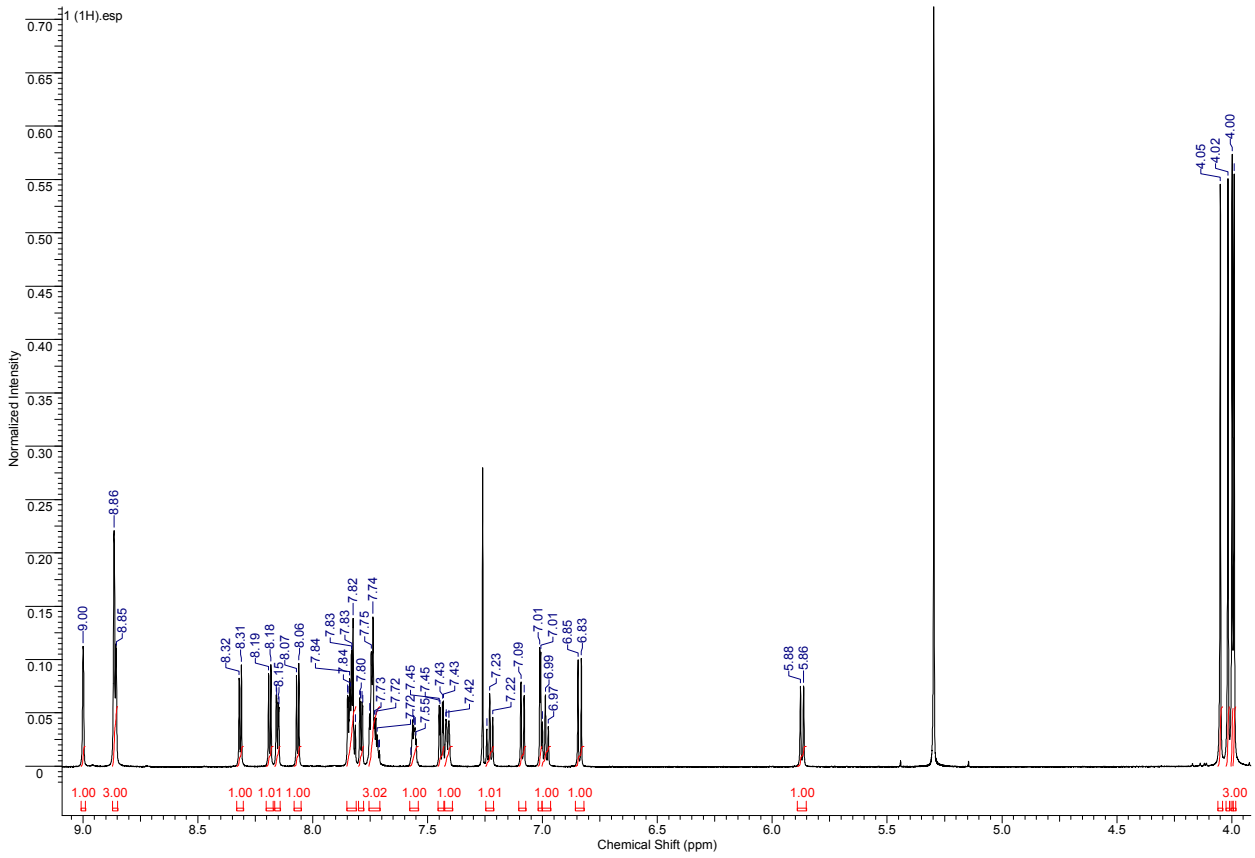

Figure S2. ^{1}H NMR spectrum of **1** (600 MHz, 298K, $CDCl_3$).

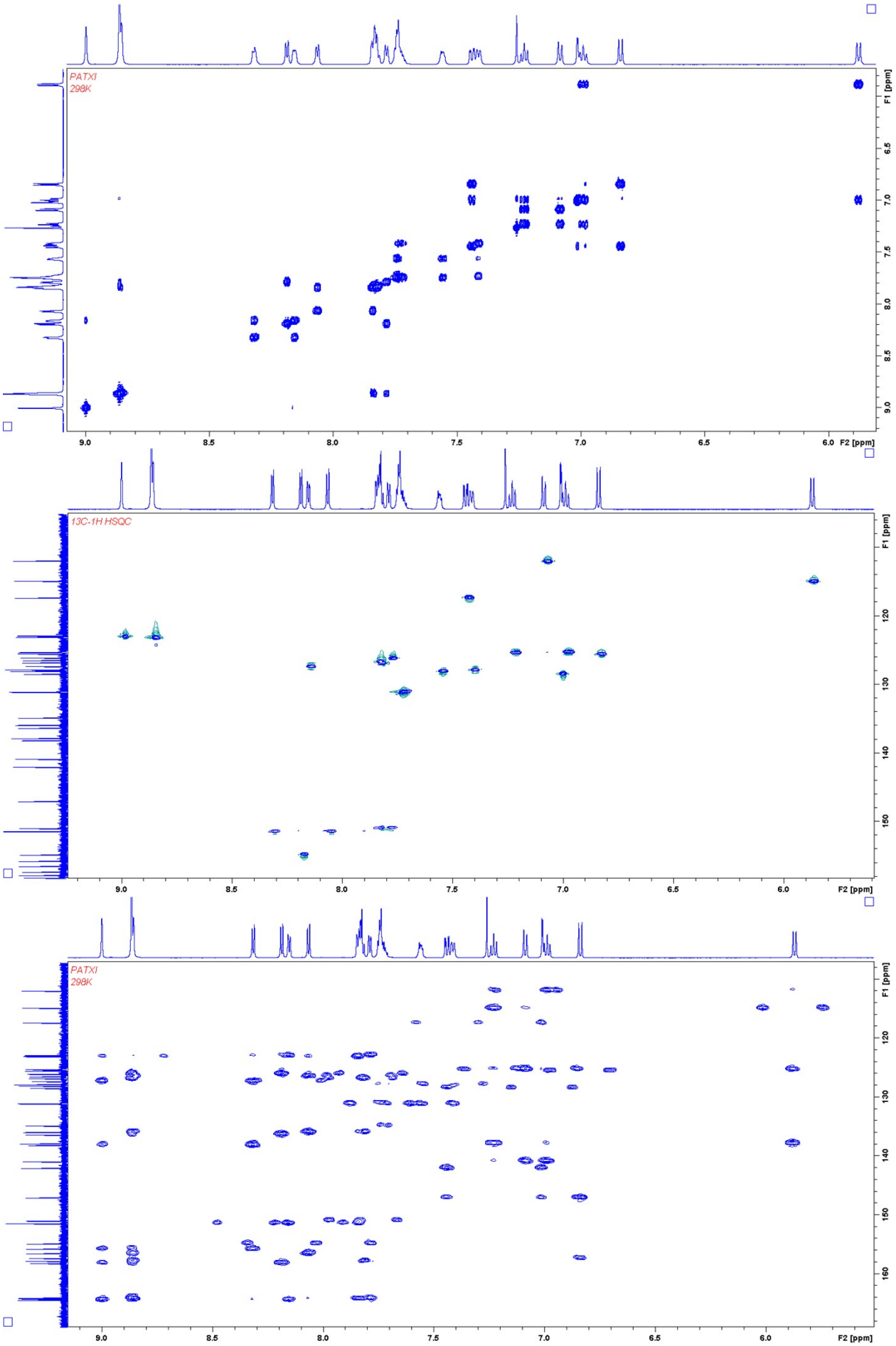

Figure S3. COSY ^{1}H,^{1}H (top); HSQC (middle); HMBC (bottom) spectra of **1**.

Assignment:

3.99 (s, 3 H), 4.00 (s, 3 H), 4.02 (s, 3 H), 4.05 (s, 3 H)	$COOCH_3$
5.87 (d, *J*=8.3 Hz, 1 H)	4
6.84 (d, *J*=8.6 Hz, 1 H)	14
6.99 (t, *J*=7.8 Hz, 1 H)	5
7.01 (d, *J*=2.2 Hz, 1 H)	13
7.09 (d, *J*=8.3 Hz, 1 H)	7
7.23 (t, *J*=7.8 Hz, 1 H)	6
7.39 - 7.43 (m, 1 H)	8 or 12
7.44 (dd, *J*=8.7, 2.3 Hz, 1 H)	15
7.54 - 7.58 (m, 1 H)	8 or 12
7.71 - 7.76 (m, 3 H)	9 + 10 + 11
7.79 (dd, *J*=6.0, 1.6 Hz, 1 H)	2
7.81 - 7.85 (m, 3 H)	2 + 2 + 1
8.07 (d, *J*=6.0 Hz, 1 H)	1
8.15 (dd, *J*=5.6, 1.4 Hz, 1 H)	2
8.19 (d, *J*=6.0 Hz, 1 H), 8.32 (d, *J*=5.6 Hz, 1 H)	1
8.85 - 8.87 (m, 3 H), 9.00 (s, 1 H)	3

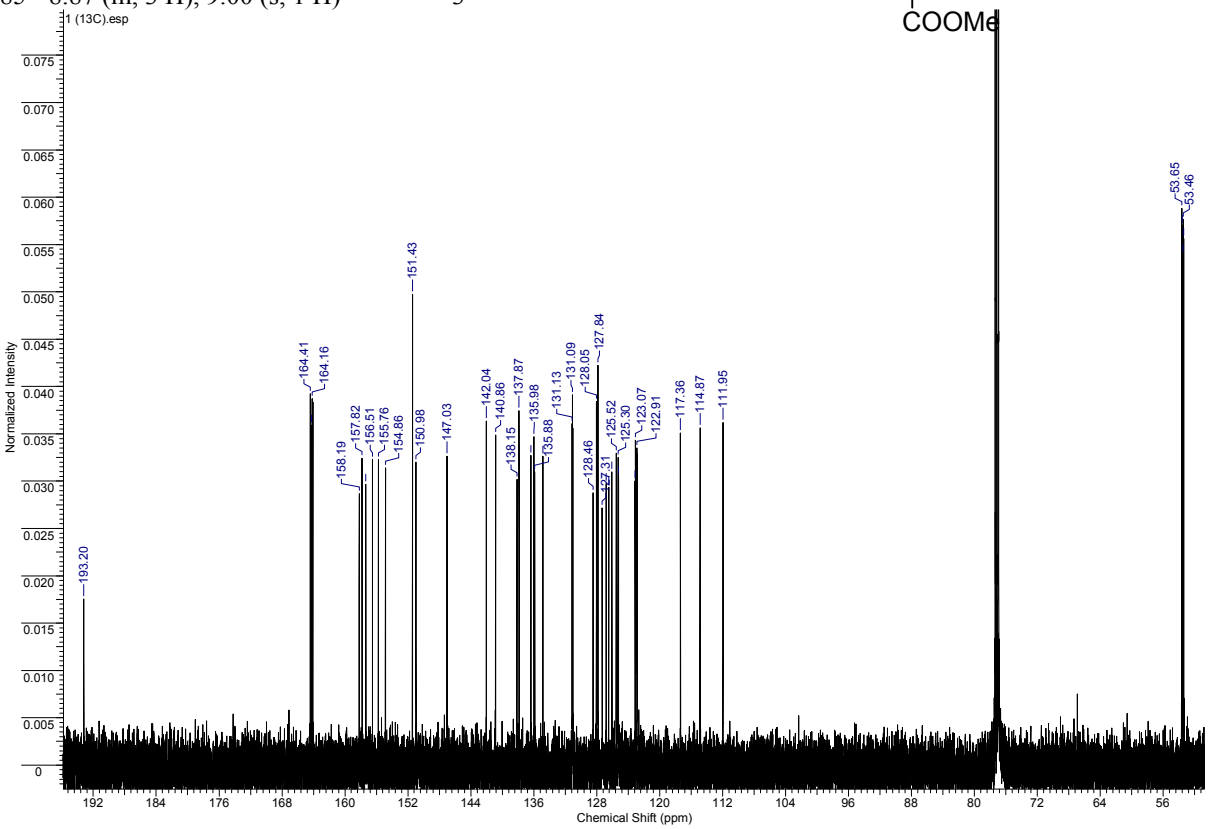

Figure S4. $^{13}C\{^{1}H\}$ NMR spectrum of **1** (151 MHz, 298K, $CDCl_3$).

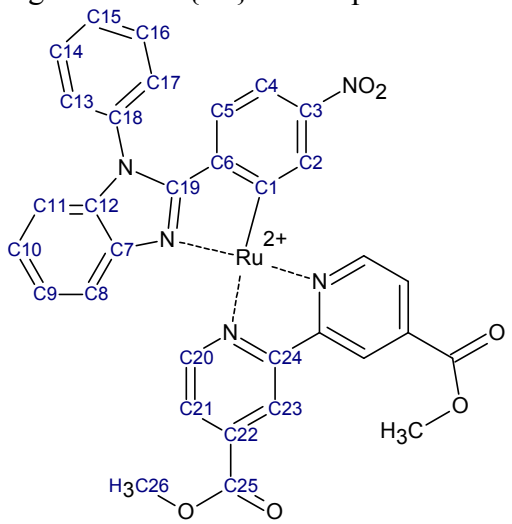

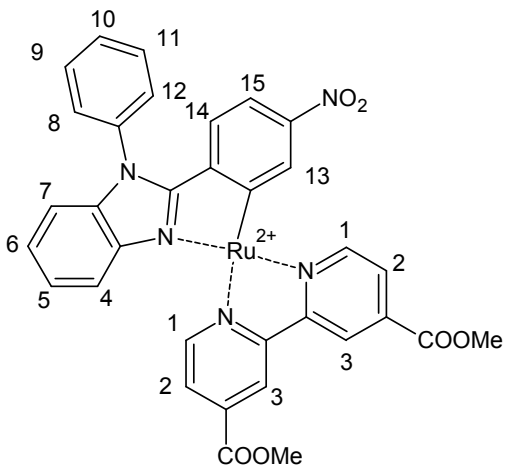

Assignment of ^{13}C and ^{1}H NMR signals to carbon and hydrogen atoms of complex **1**. Carbon and hydrogen atoms labeling is shown at the above figures.

Carbon	^{13}C δ, ppm	^{1}H δ, ppm	Hydrogen
C1	193.2	-	-
C2	128.5	7.01	13
C3	157.4	-	-
C4	117.4	7.44	15
C5	125.5	6.84	14
C6	142.0	-	-
C7	140.9	-	-
C8	114.9	5.87	4
C9	125.2	6.99	5
C10	125.3	7.23	6
C11	112.0	7.09	7
C12	137.9	-	-
C13/C17	127.8/128.1	7.39-7.43/7.54-7.58	8 or 12
C14	131.0		
C15	131.1		
C16	131.1	7.71 – 7.76	9, 10, 11
C17/C13	127.8/128.1	7.39-7.43/7.54-7.58	8 or 12
C18	134.8	-	-
C19	147.0	-	-
C20	126.1 126.5 126.8 127.3	7.79 7.81-7.85 8.15	2
C21	151.0 151.4 151.4 154.9	7.82 8.07 8.32 8.19	1
C22	135.9 136.0 136.4 138.2	-	-
C23	122.9 122.9 123.1 123.1	8.85-8.87 9.00	3
C24	155.8 156.5 157.8 158.2	-	-
C25	164.1 164.2 164.3 164.4	-	-
C26	53.4 53.5 53.6 53.7	3.99 4.00 4.02 4.05	-COO*CH₃*

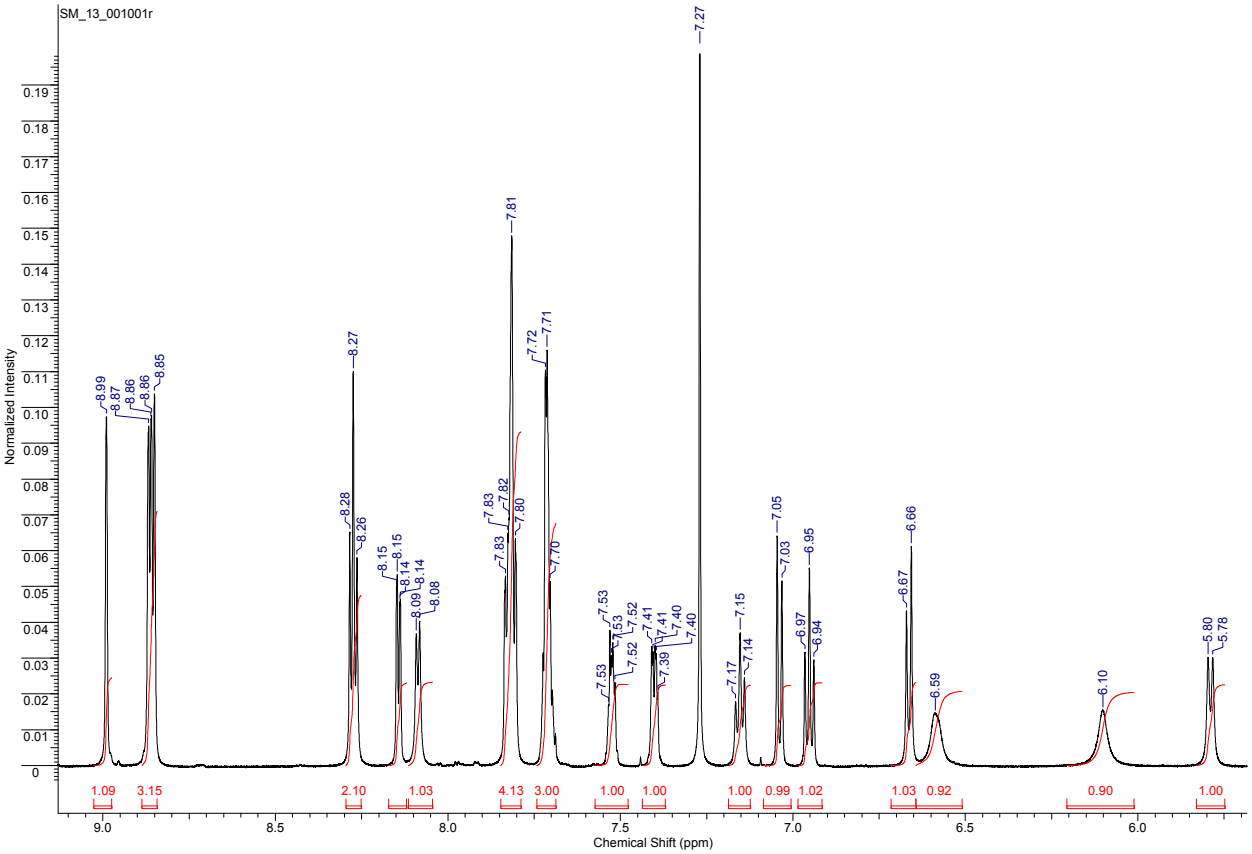

Figure S5. Aromatic region of ^{1}H NMR spectrum of **2** (600 MHz, 298K, $CDCl_3$).

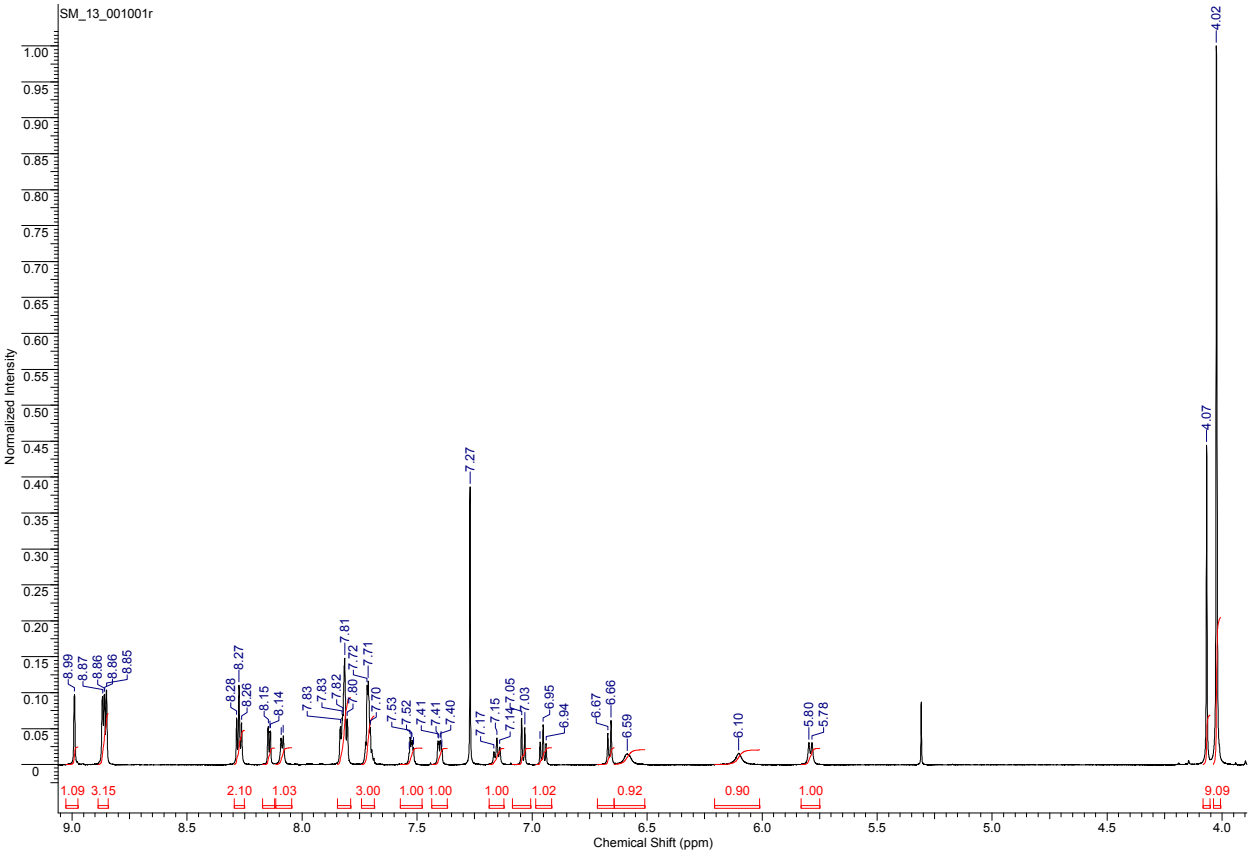

Figure S6. ^{1}H NMR spectrum of **2** (600 MHz, 298K, $CDCl_3$).

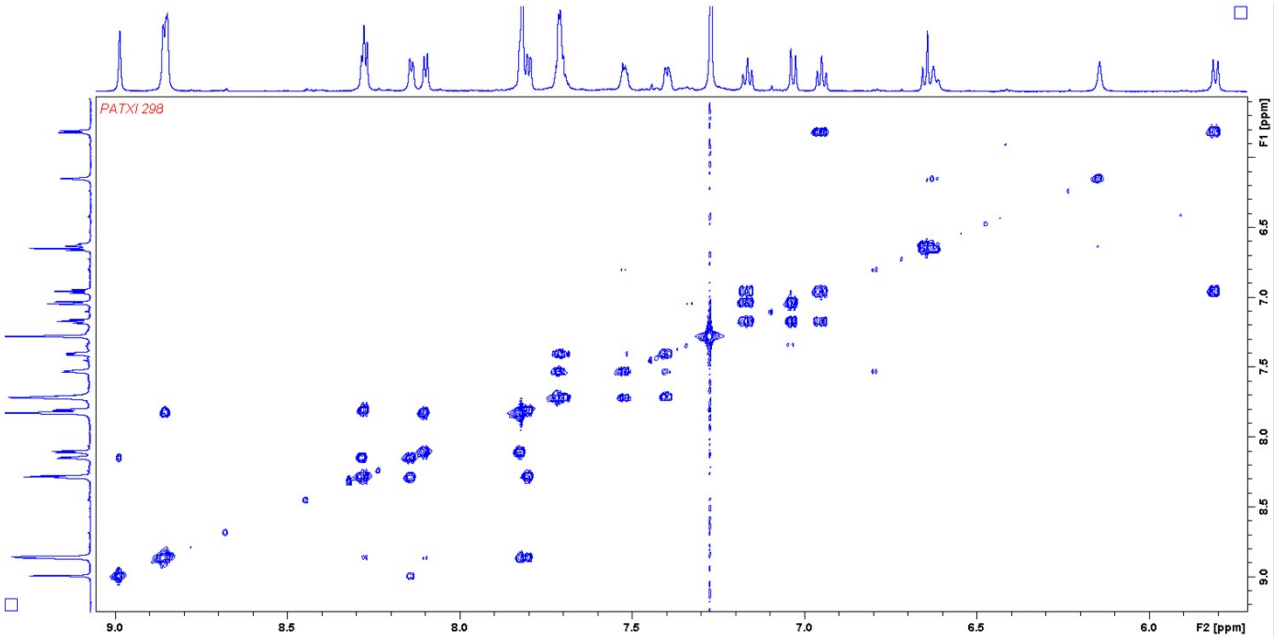

Figure S7. COSY ^{1}H,^{1}H spectrum of **2**.

Assignment:	
4.02 (s, 9 H)	COOMe
4.07 (s, 3 H)	COOMe
5.78 (d, *J*=8.4 Hz, 1 H)	4
6.04-6.15 (m, 1H)	13
6.55 - 6.66 (m, 2 H)	14 + 15
6.95 (t, *J*=8.4 Hz, 1 H)	5
7.04 (d, *J*=8.3 Hz, 1 H)	7
7.12 - 7.19 (m, 1 H)	6
7.37 - 7.43 (m, 1 H)	8 or 12
7.50 - 7.55 (m, 1 H)	8 or 12
7.67 - 7.75 (m, 3 H)	9 + 10 + 11
7.78 - 7.86 (m, 4 H)	1 + 1 + 2 + 2
8.09 (d, *J*=6.4 Hz, 1 H)	2
8.15 (dd, J_1=5.8 Hz, J_2=1.2 Hz, 1H)	2
8.27 (m, 2 H)	1 + 1
8.84 - 8.88 (m, 3 H)	3 + 3 + 3
8.99 (s, 1 H)	3

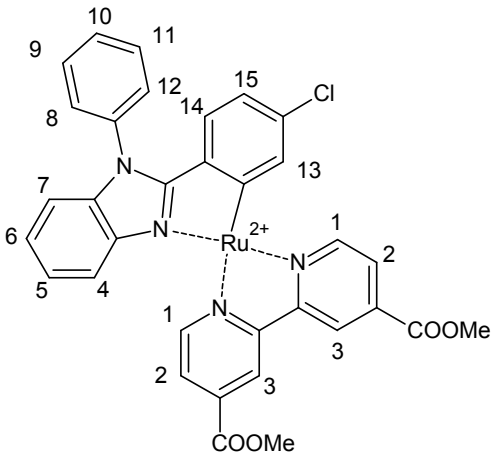

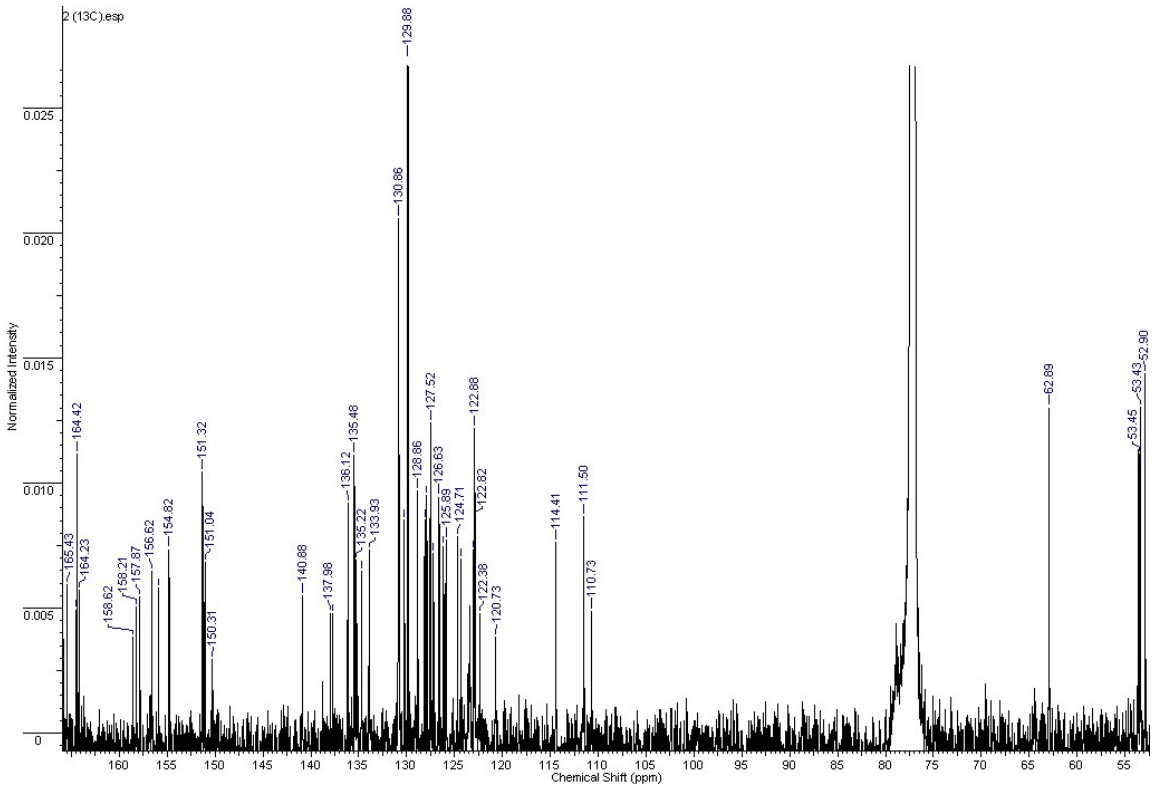

Figure S8. $^{13}C\{^{1}H\}$ NMR spectrum of **2** (151 MHz, 298K, $CDCl_3$).

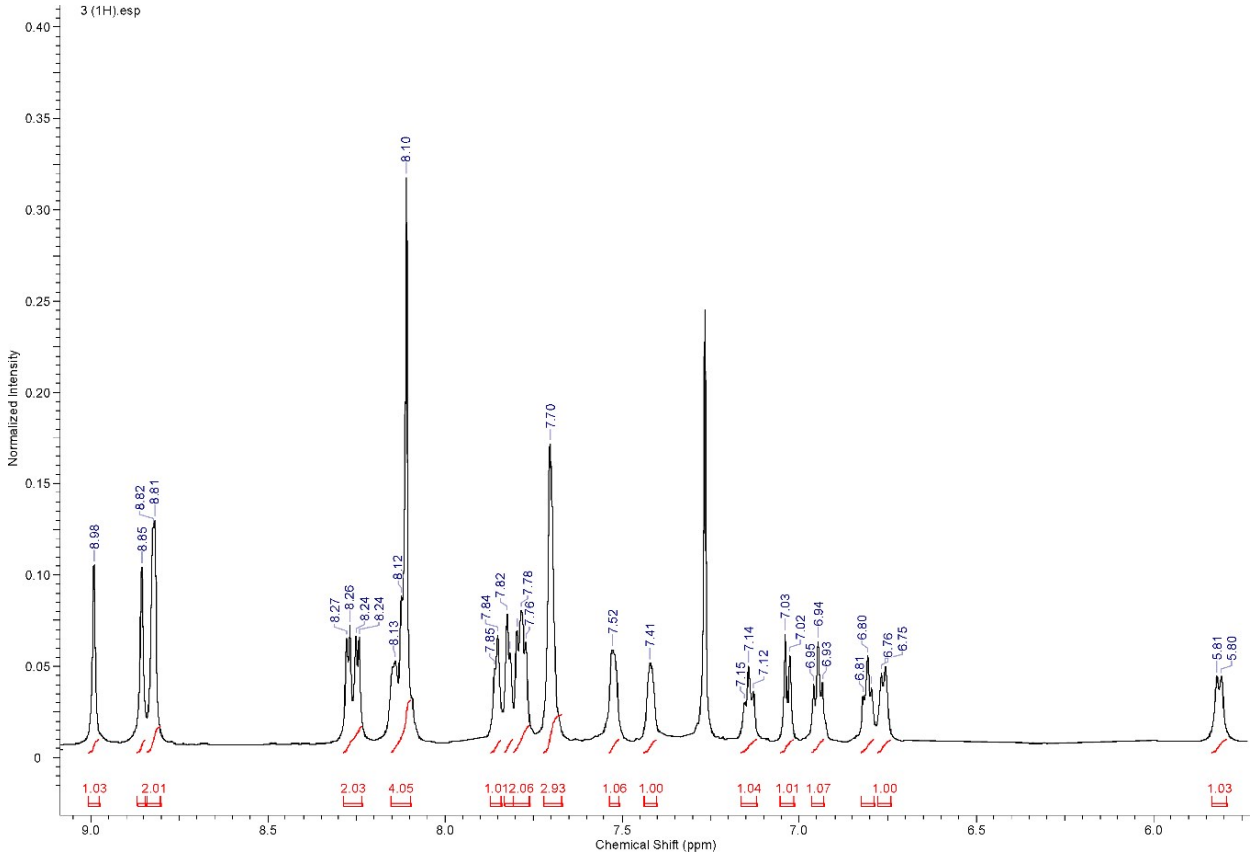

Figure S9. Aromatic region of ^{1}H NMR spectrum of **3** (600 MHz, 298K, $CDCl_3$).

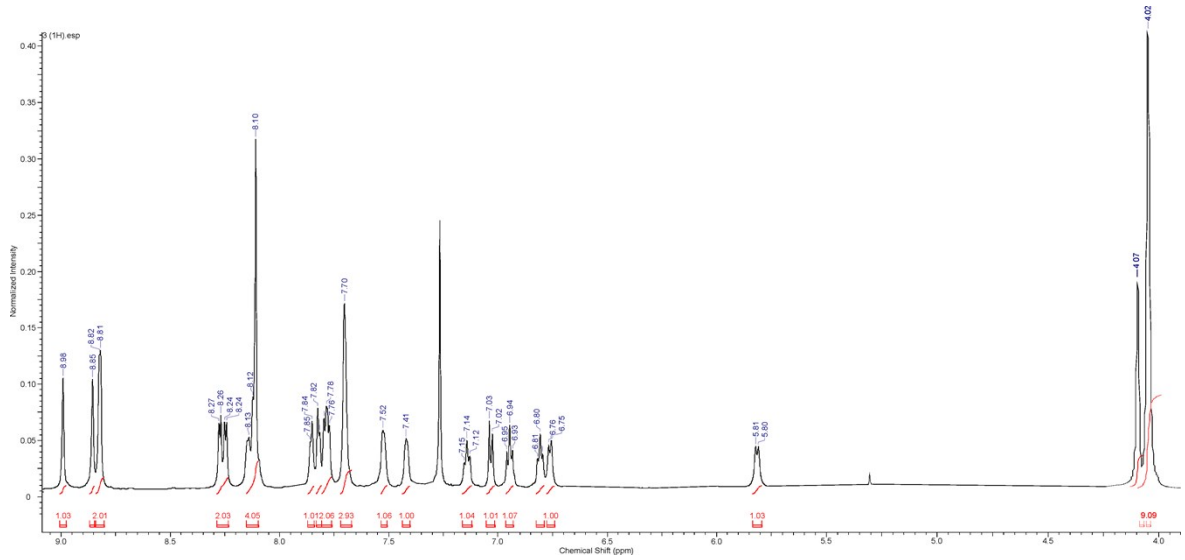

Figure S10. ^{1}H NMR spectrum of **3** (600 MHz, 298K, $CDCl_3$).

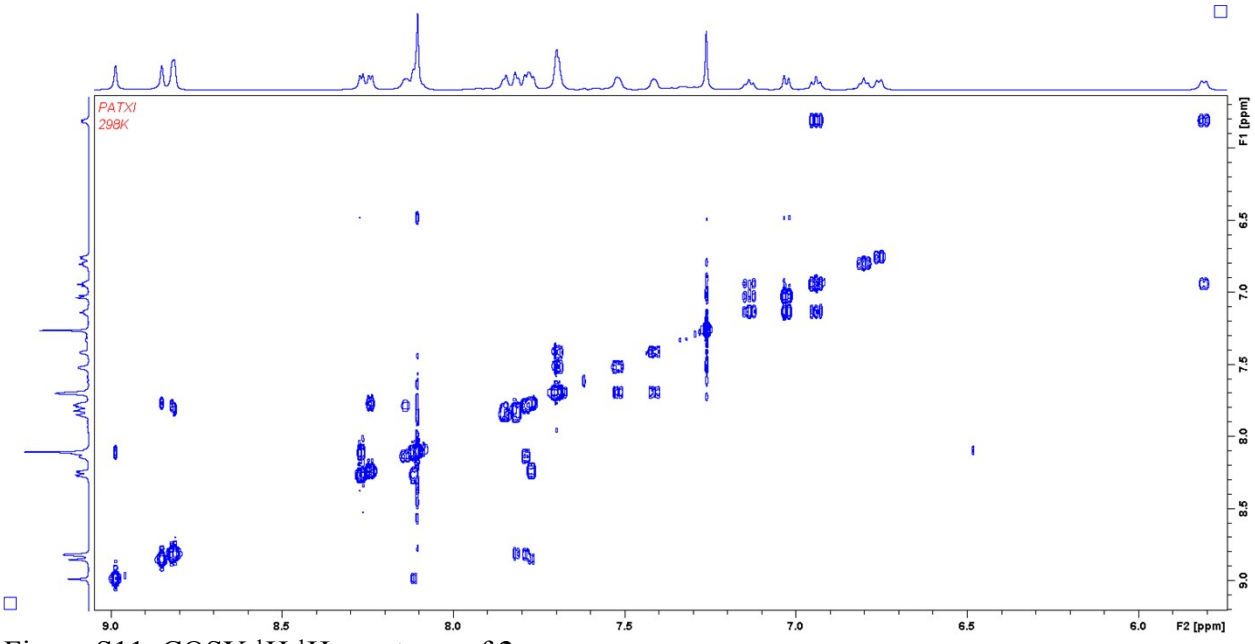

Figure S11. COSY ^{1}H,^{1}H spectrum of **3**.

Assignment:	
4.02 (s, 9 H)	COOMe
4.07 (s, 3 H)	COOMe
5.81 (d, *J*=7.6 Hz, 1 H)	4
6.76 (d, *J*=7.3 Hz, 1 H)	13
6.80 (t, *J*=7.0 Hz, 1 H)	14
6.94 (t, *J*=7.56 Hz, 1 H)	5
7.03 (d, *J*=8.1 Hz, 1 H)	7
7.14 (t, *J*=7.3 Hz, 1 H)	6
7.41 (m, 1 H)	8 or 12
7.52 (m, 1 H)	8 or 12
7.70 (m, 3 H)	9 + 10 + 11
7.76 - 7.80 (m, 2 H)	2 + 2
7.81 (d, *J*=5.3 Hz, 1 H)	2
7.85 (d, *J*=5.0 Hz, 1 H)	2
8.09 - 8.14 (m, 4 H)	1 + 1 + 15 + 16
8.25 (m, 2 H)	1 + 1
8.82 (m, 2 H)	3 + 3
8.85 (s, 1 H)	3
8.98 (s, 1 H)	3

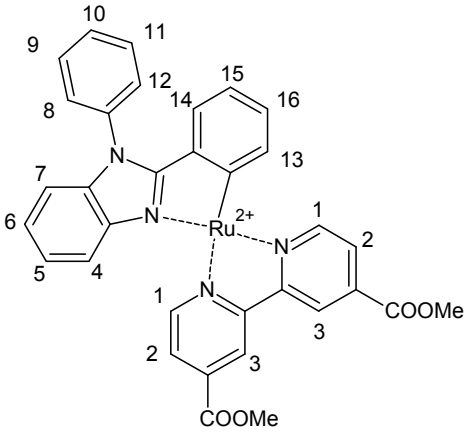

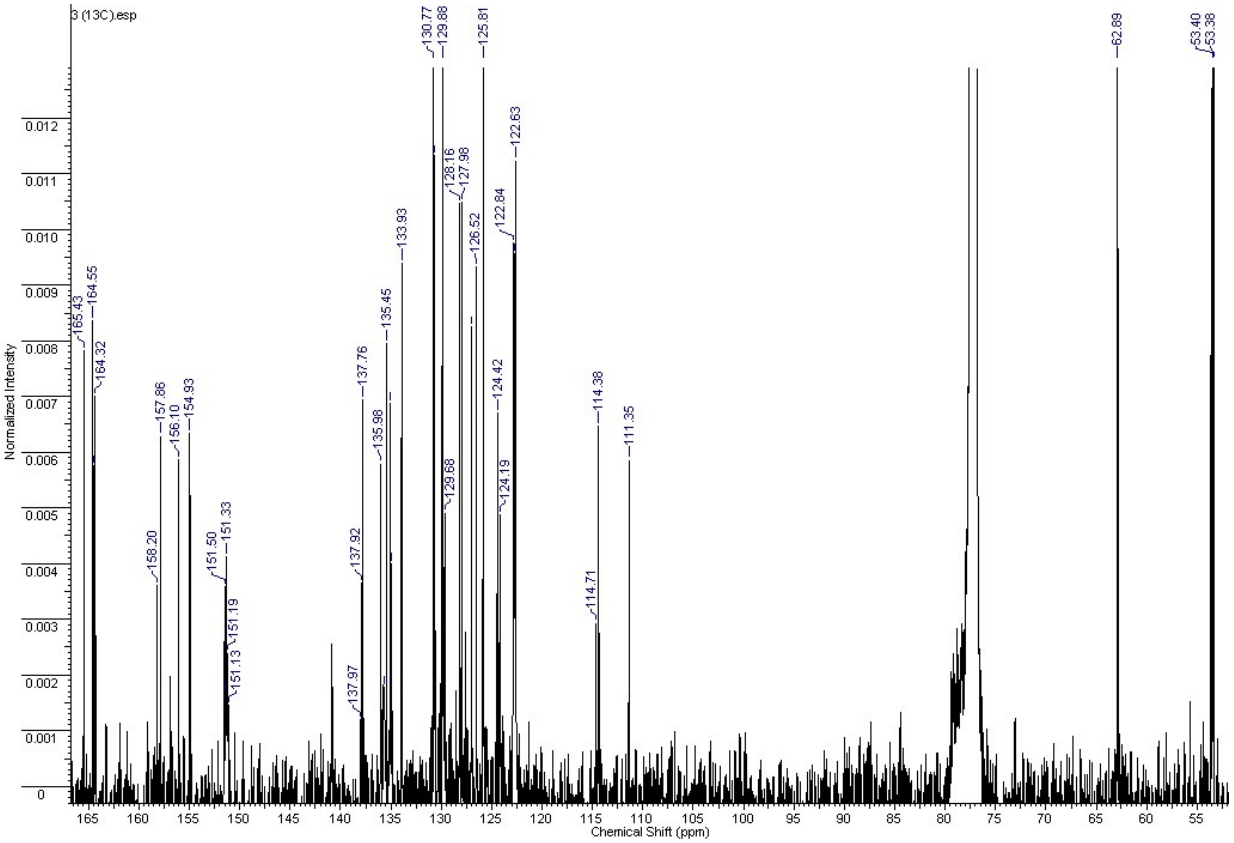

Figure S12. $^{13}C\{^{1}H\}$ NMR spectrum of **3** (151 MHz, 298K, $CDCl_3$).

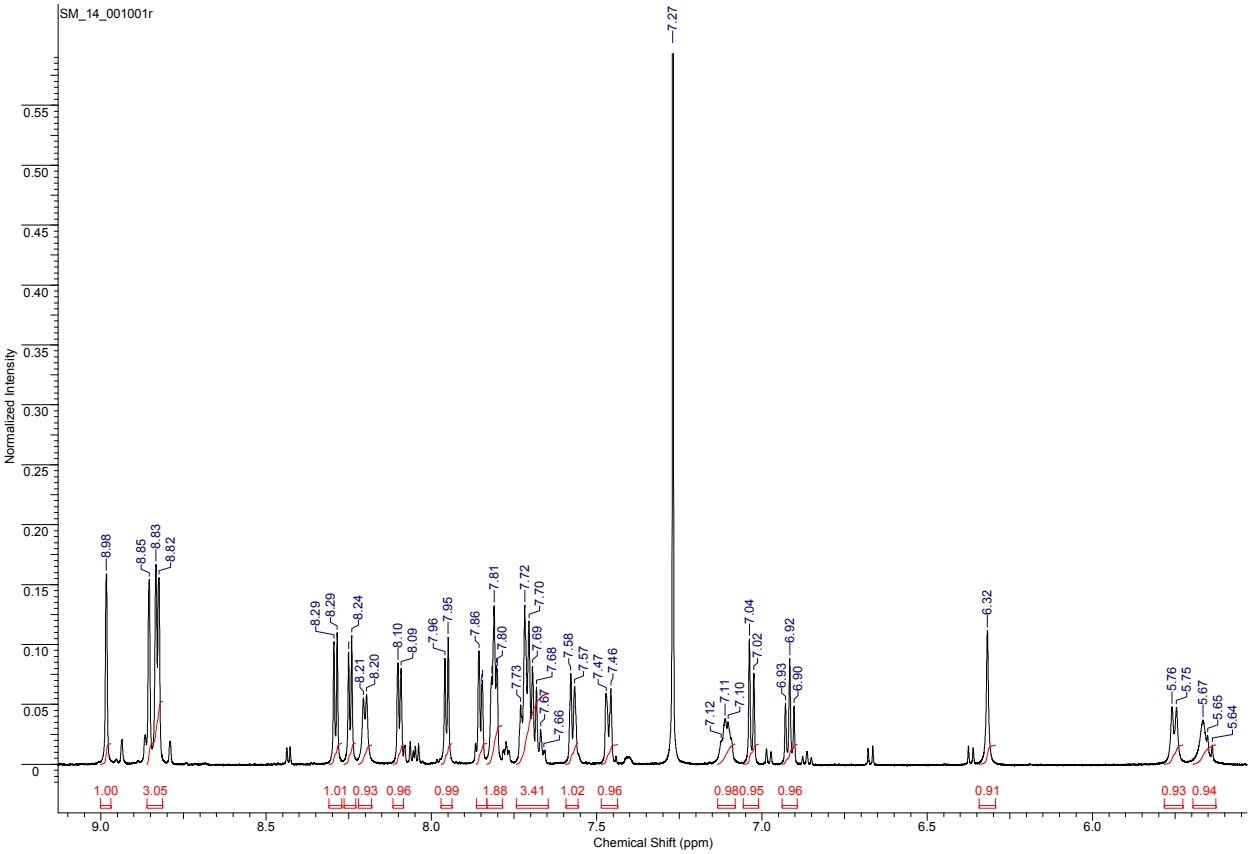

Figure S13. Aromatic region of ^{1}H NMR spectrum of **4** (600 MHz, 298K, $CDCl_3$).

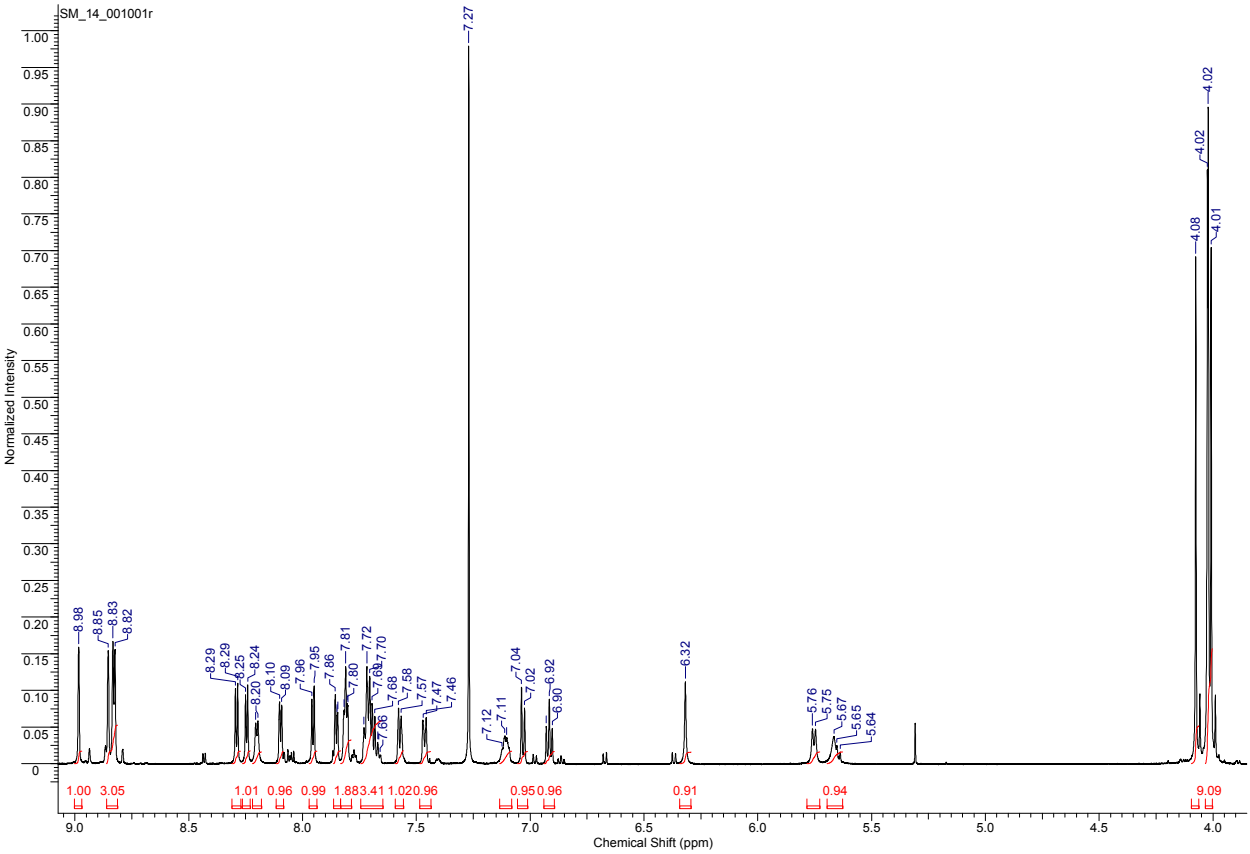

Figure S14. ^{1}H NMR spectrum of **4** (600 MHz, 298K, $CDCl_3$).

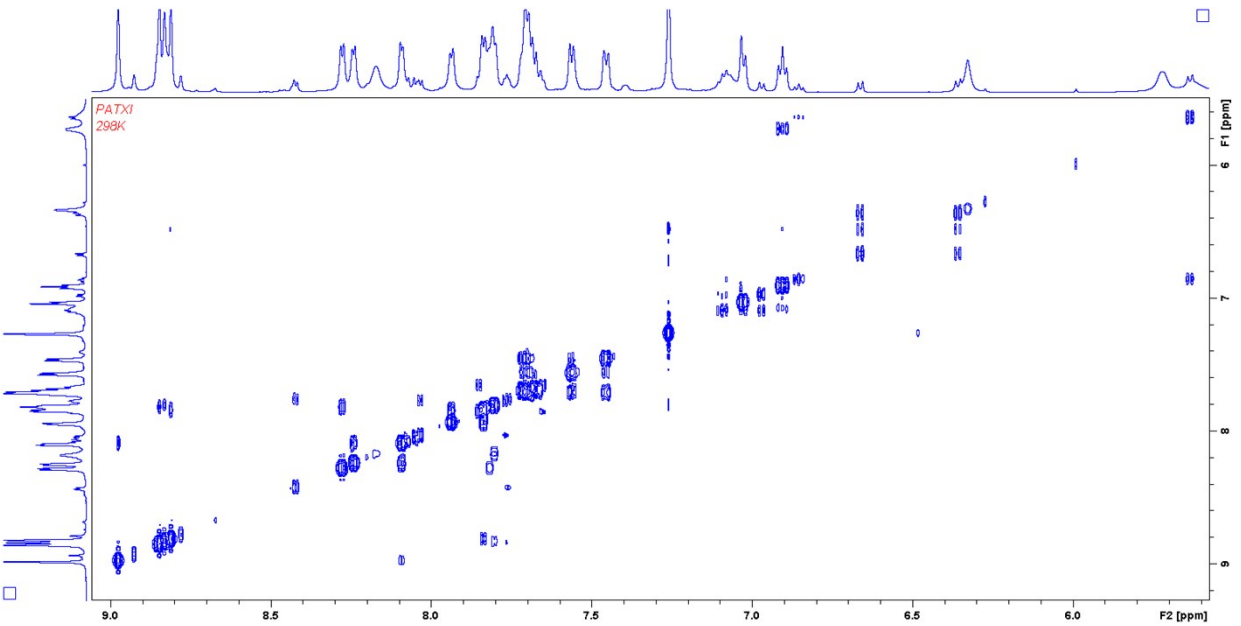

Figure S15. COSY $^{1}H,^{1}H$ spectrum of **4.**

Assignment:

3.30 (s, 3H)	OMe
3.42 (s, 3H)	OMe
4.02 (s, 9 H)	COOMe
4.08 (s, 3 H)	COOMe
5.63 - 5.70 (m, 1 H)	13
5.76 (d, *J*=8.0 Hz, 1 H)	4
6.32 (s, 1 H)	14

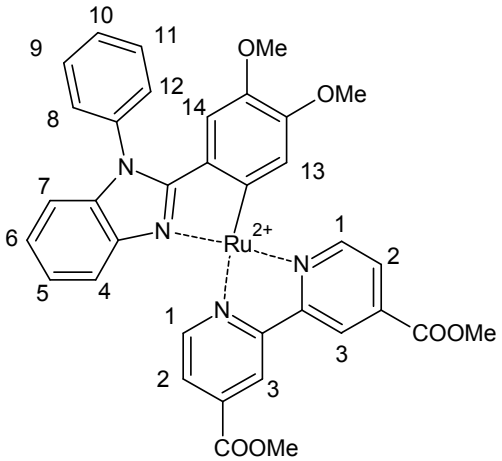

6.92 (t, *J*=8.0 Hz, 1 H)	5
7.03 (d, *J*=8.1 Hz, 1 H)	7
7.08 - 7.14 (m, 1 H)	6
7.46 (d, *J*=9.7 Hz, 1 H)	8 or 12
7.57 (d, *J*=7.0 Hz, 1 H)	8 or 12
7.65 - 7.75 (m, 3 H)	9 + 10 + 11
7.79 - 7.83 (m, 2 H)	2 + 2
7.84 - 7.87 (m, 1 H)	1
7.95 (d, *J*=5.7 Hz, 1 H)	1
8.10 (d, *J*=5.7 Hz, 1 H)	2
8.21 (d, *J*=6.0 Hz, 1 H)	2
8.25 (d, *J*=5.6 Hz, 1 H)	1
8.29 (d, *J*=5.9 Hz, 1 H)	1
8.80 - 8.88 (m, 3 H)	3 + 3 + 3
8.98 (s, 1 H)	3

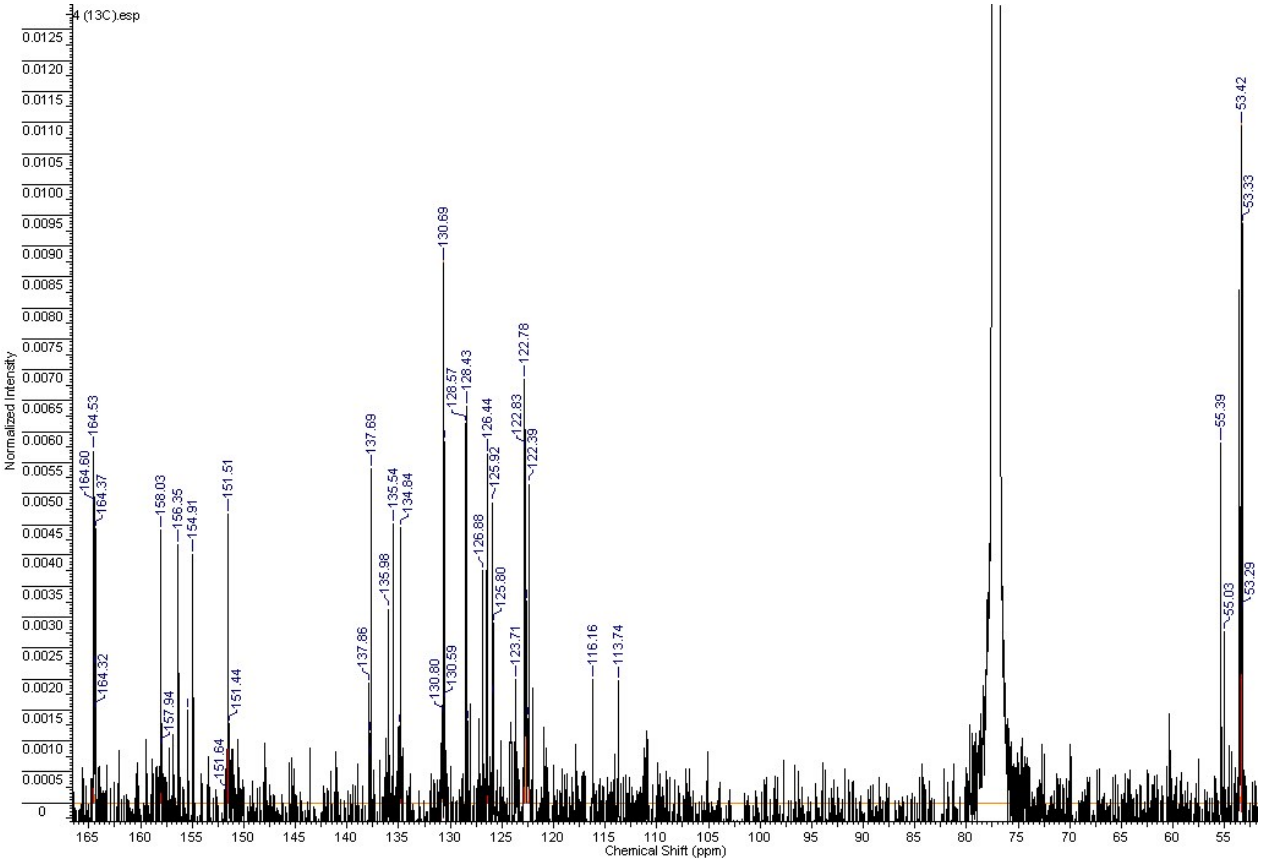

Figure S16. $^{13}C\{^{1}H\}$ NMR spectrum of **4** (151 MHz, 298K, $CDCl_3$).

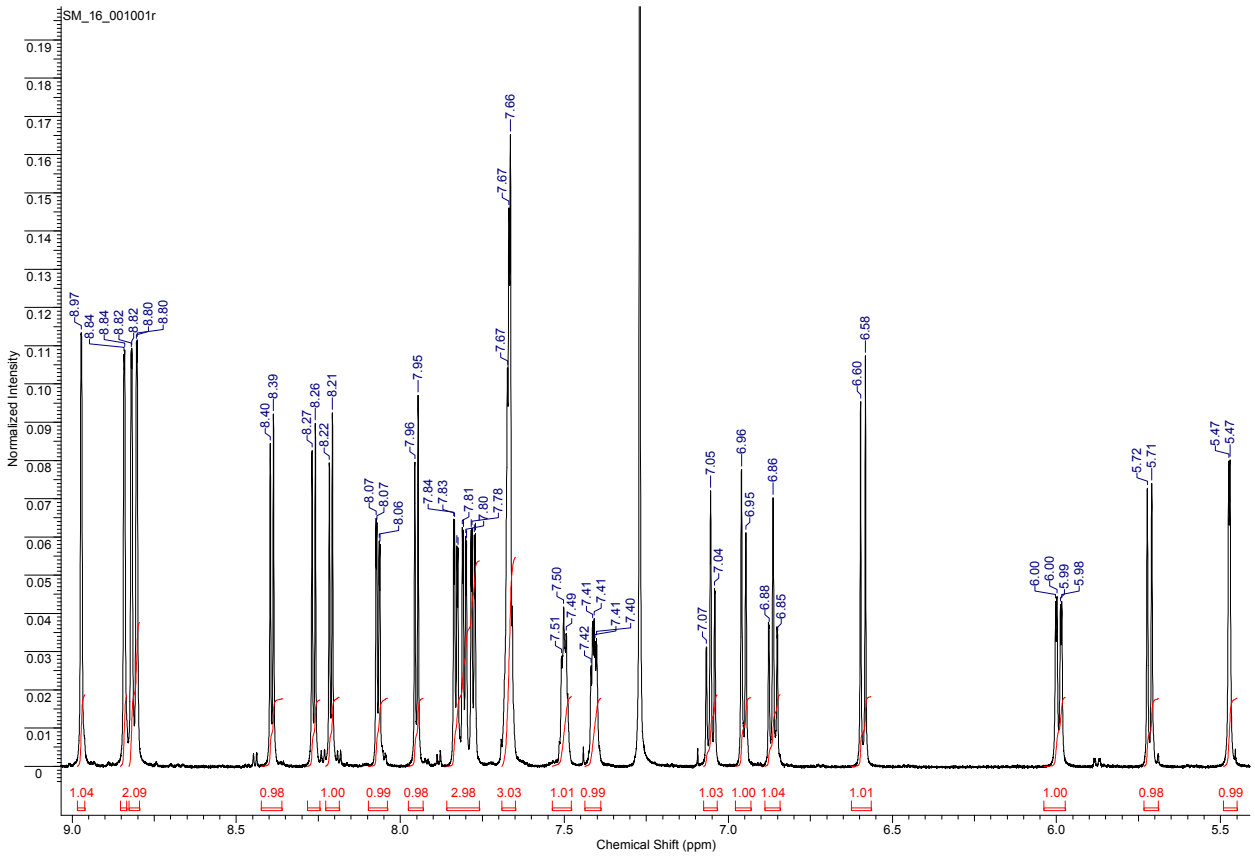

Figure S17. Aromatic region of ^{1}H NMR spectrum of **5** (600 MHz, 298K, $CDCl_3$).

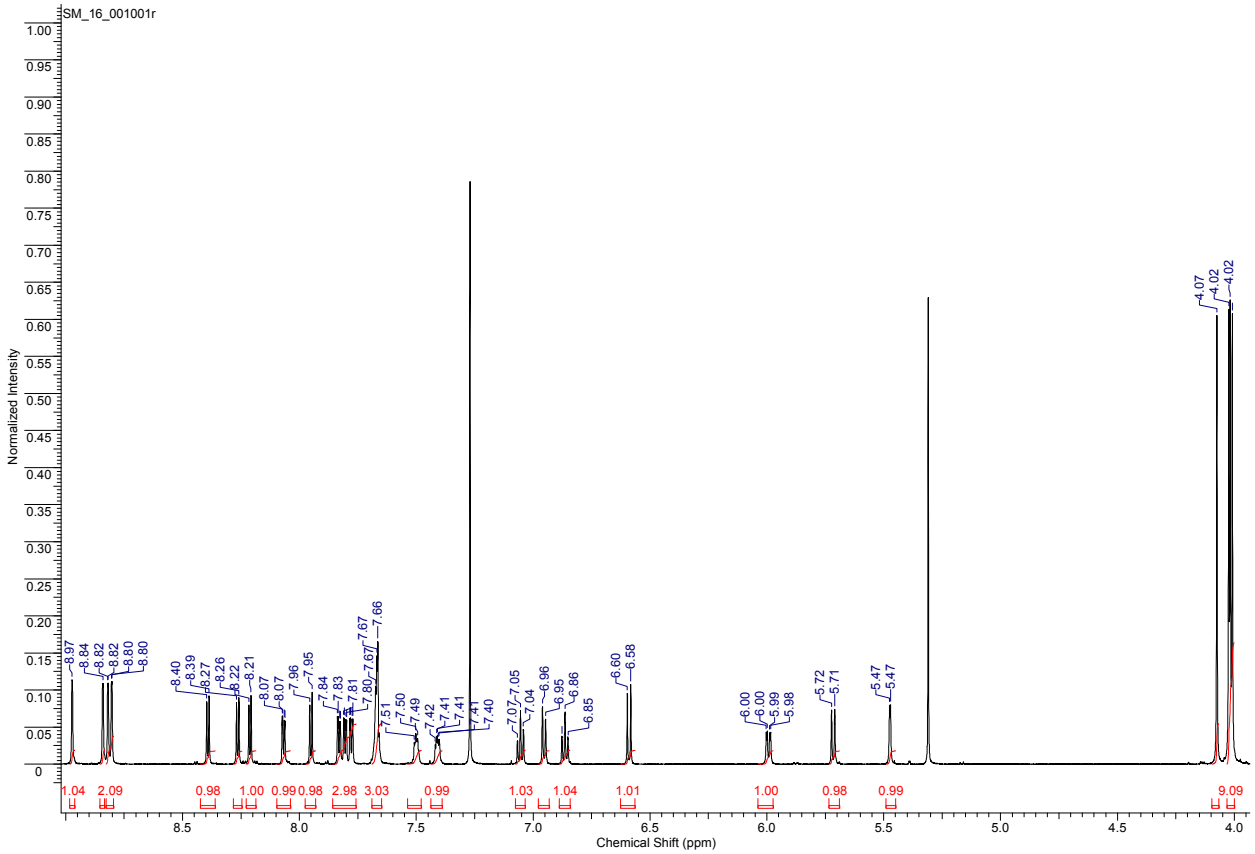

Figure S18. ^{1}H NMR spectrum of **5** (600 MHz, 298K, $CDCl_3$).

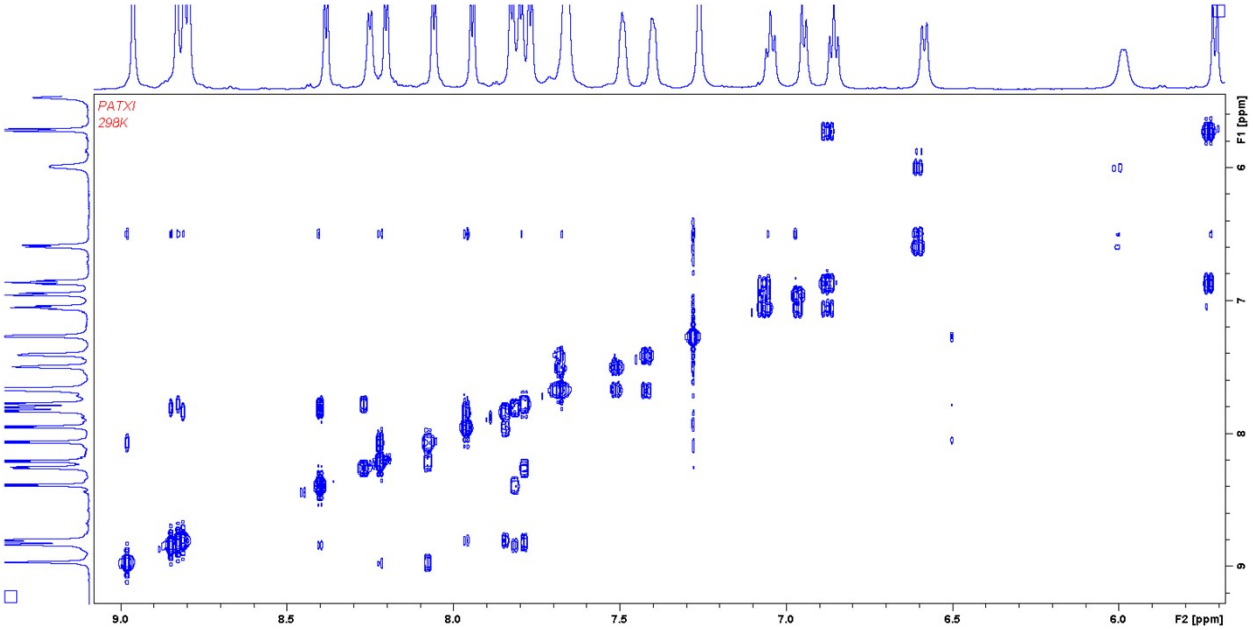

Figure S19. COSY $^{1}H,^{1}H$ spectrum of **5.**

Assignment:

2.64 (s., 6 H)	NMe_2
4.02 (s, 9 H)	COOMe
4.07 (s, 3 H)	COOMe
5.47 (d, *J*=2.2 Hz, 1 H)	13
5.72 (d, *J*=8.1 Hz, 1 H)	4
5.99 (dd, J_1=8.7 Hz, J_2=2.5 Hz, 1 H)	15
6.59 (d, *J*=8.8 Hz, 1 H)	14
6.86 (t, *J*=7.2 Hz, 1 H)	5
6.95 (d, *J*=8.0 Hz, 1 H)	7
7.05 (t, *J*=7.7 Hz, 1 H)	6
7.39 - 7.43 (m, 1 H)	8 or 12
7.48 - 7.52 (m, 1 H)	8 or 12
7.65 - 7.70 (m, 3 H)	9 + 10 + 11
7.78 (dd, J_1=6.0 Hz, J_2=1.8 Hz, 1 H)	2
7.80 (dd, J_1=6.0 Hz, J_2=1.7 Hz, 1 H)	2
7.83 (dd, J_1=6.0 Hz, J_2=1.8 Hz, 1 H)	2
7.95 (d, *J*=6.0 Hz, 1 H)	1
8.07 (dd, J_1=5.7 Hz, J_2=1.5 Hz, 1 H)	1
8.21 (d, *J*=5.6 Hz, 1 H)	1
8.26 (d, *J*=5.9 Hz, 1 H)	2
8.38 (d, *J*=5.9 Hz, 1 H)	1
8.79 - 8.84 (m, 3 H)	3 + 3 + 3
8.97 (s, 1 H).	3

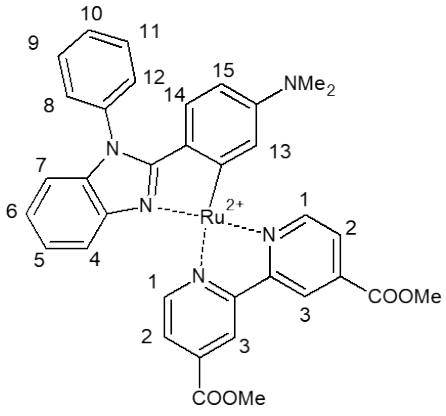

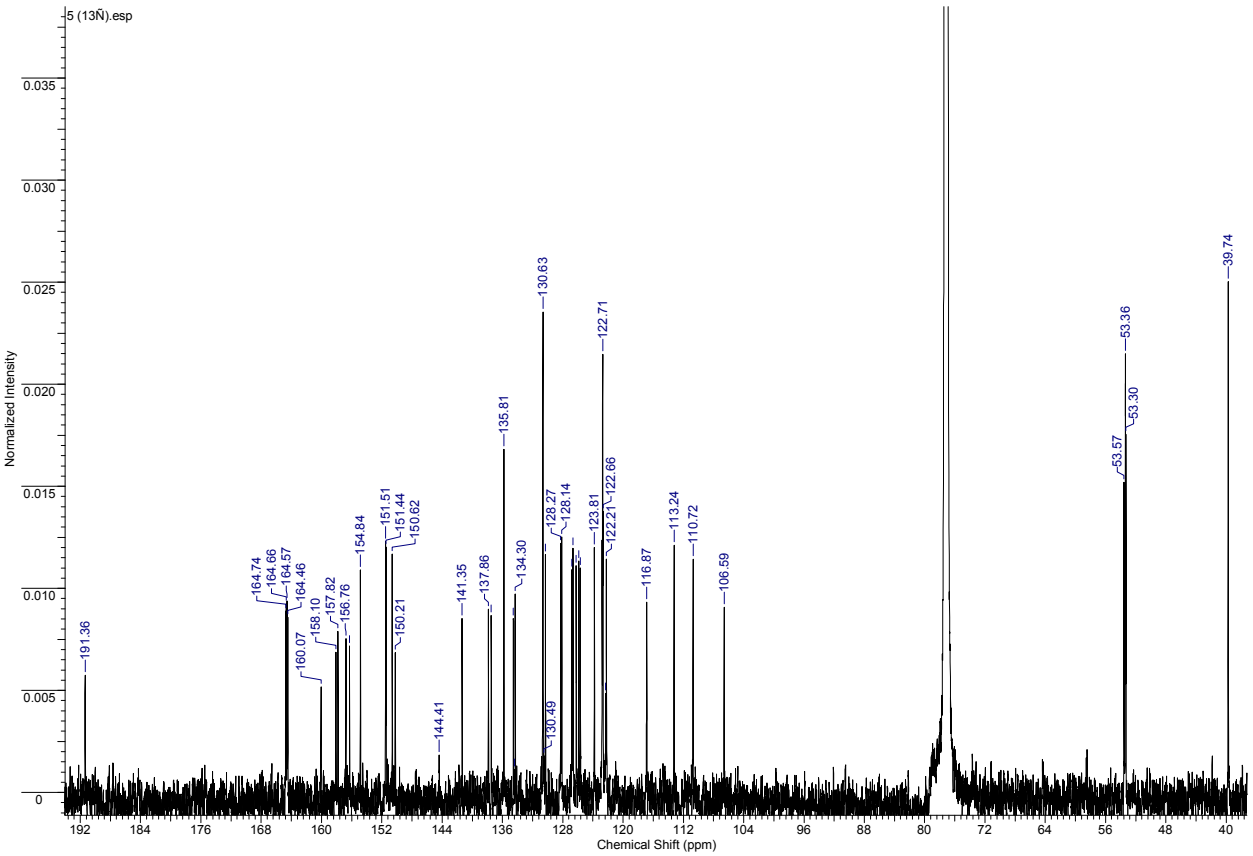

Figure S20. $^{13}C\{^{1}H\}$ NMR spectrum of **5** (151 MHz, 298K, $CDCl_3$).

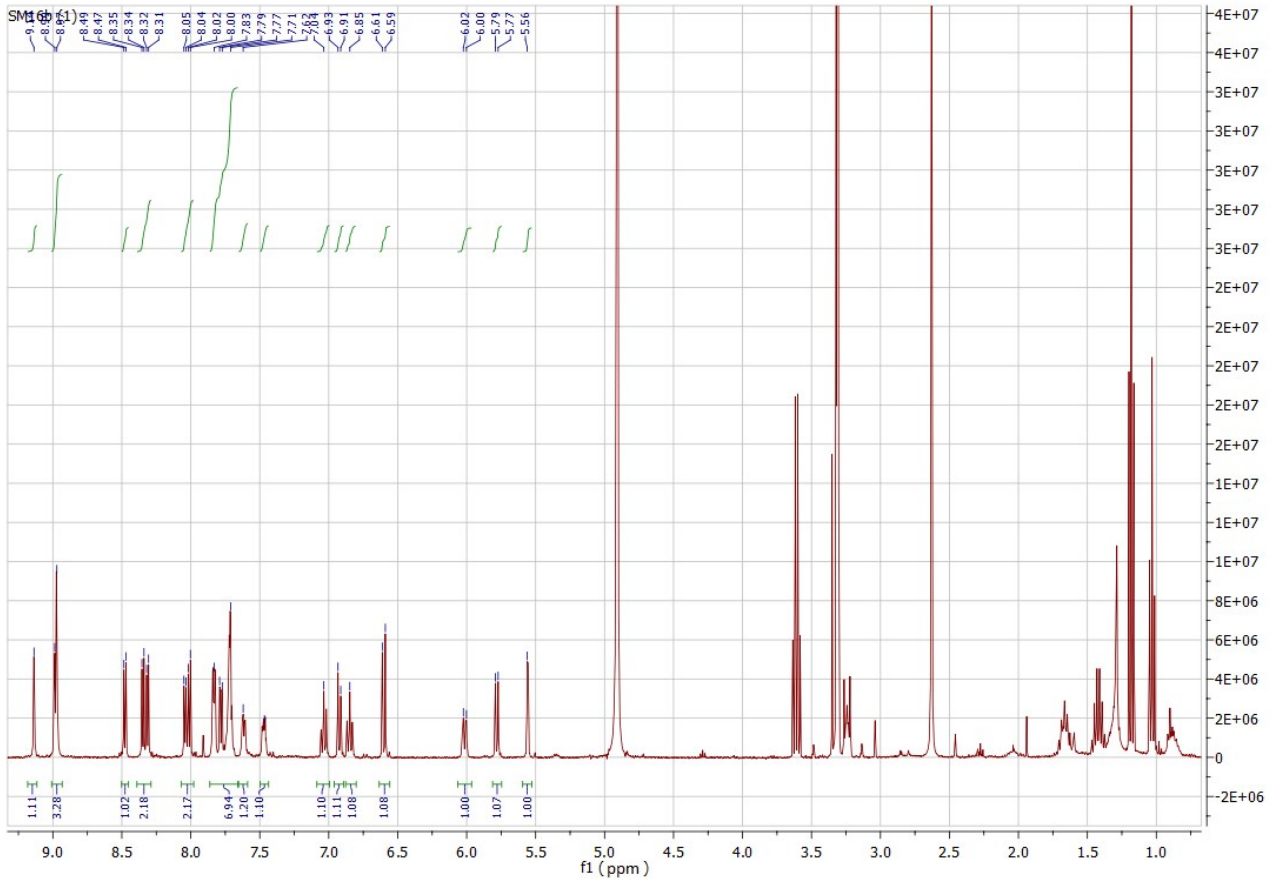

Figure S21. ^{1}H NMR spectrum of **5** after hydrolysis (400 MHz, 298K, CD_3OD).

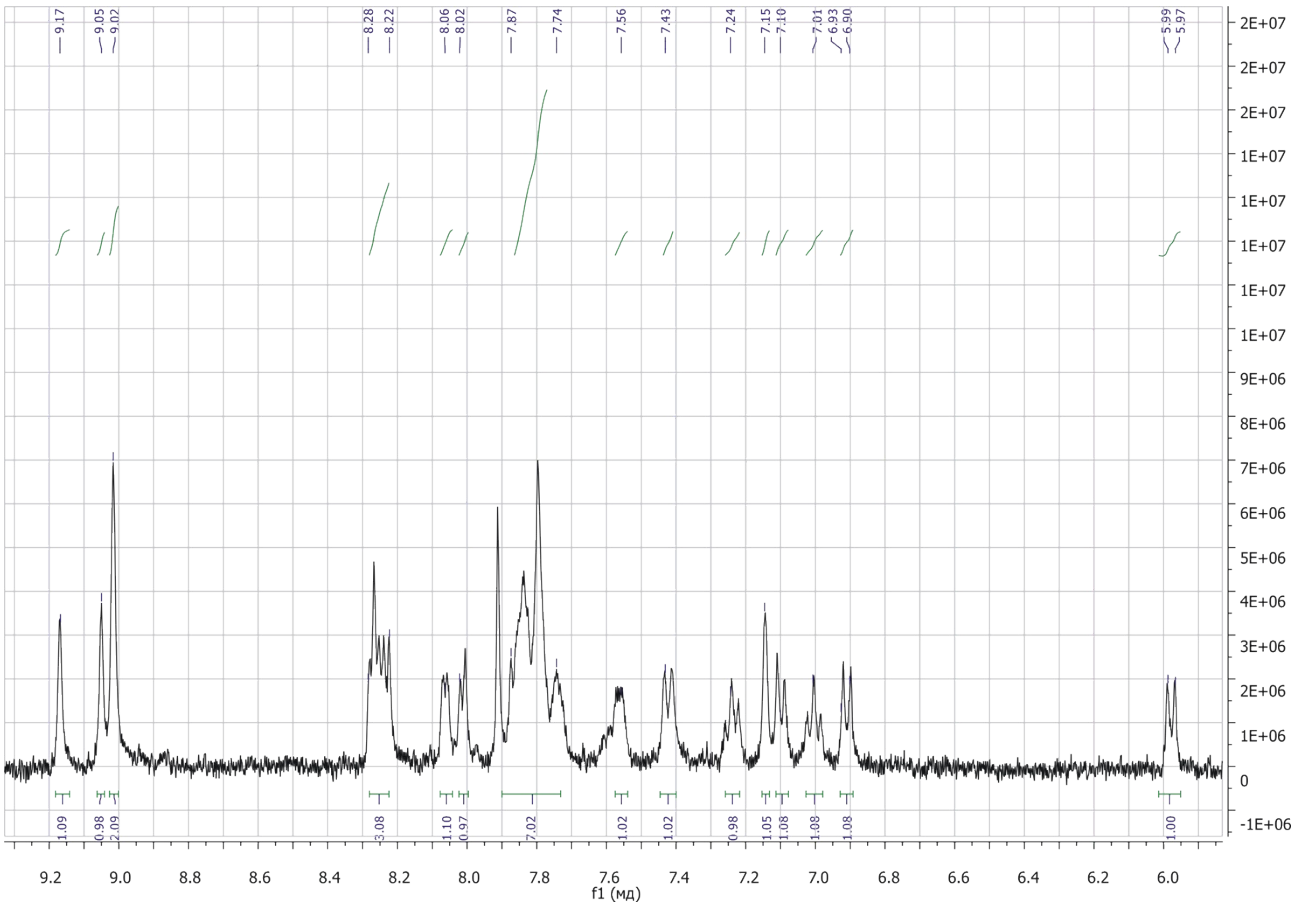

Figure S22. ^{1}H NMR spectrum of **1** after hydrolysis (400 MHz, 298K, CD_3OD).

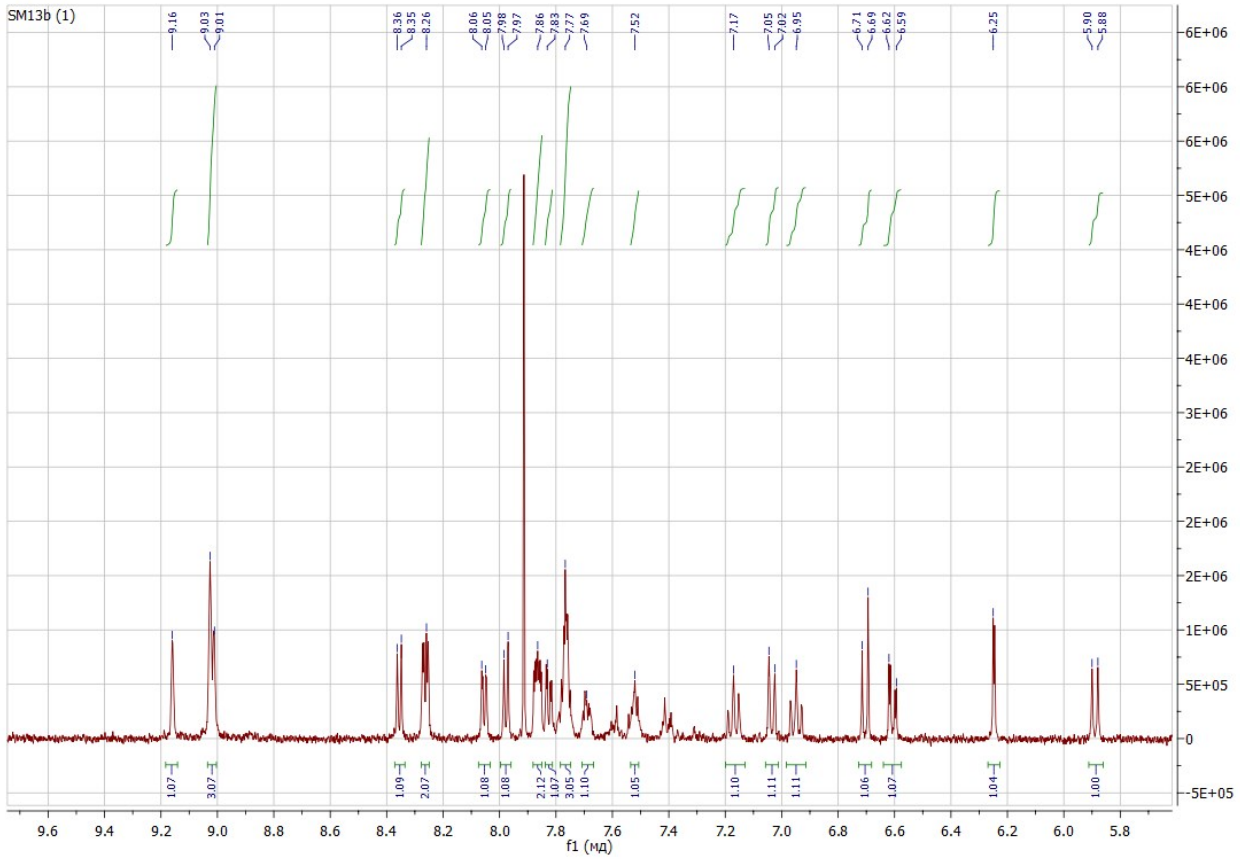

Figure S23. ^{1}H NMR spectrum of **2** after hydrolysis (400 MHz, 298K, CD_3OD).

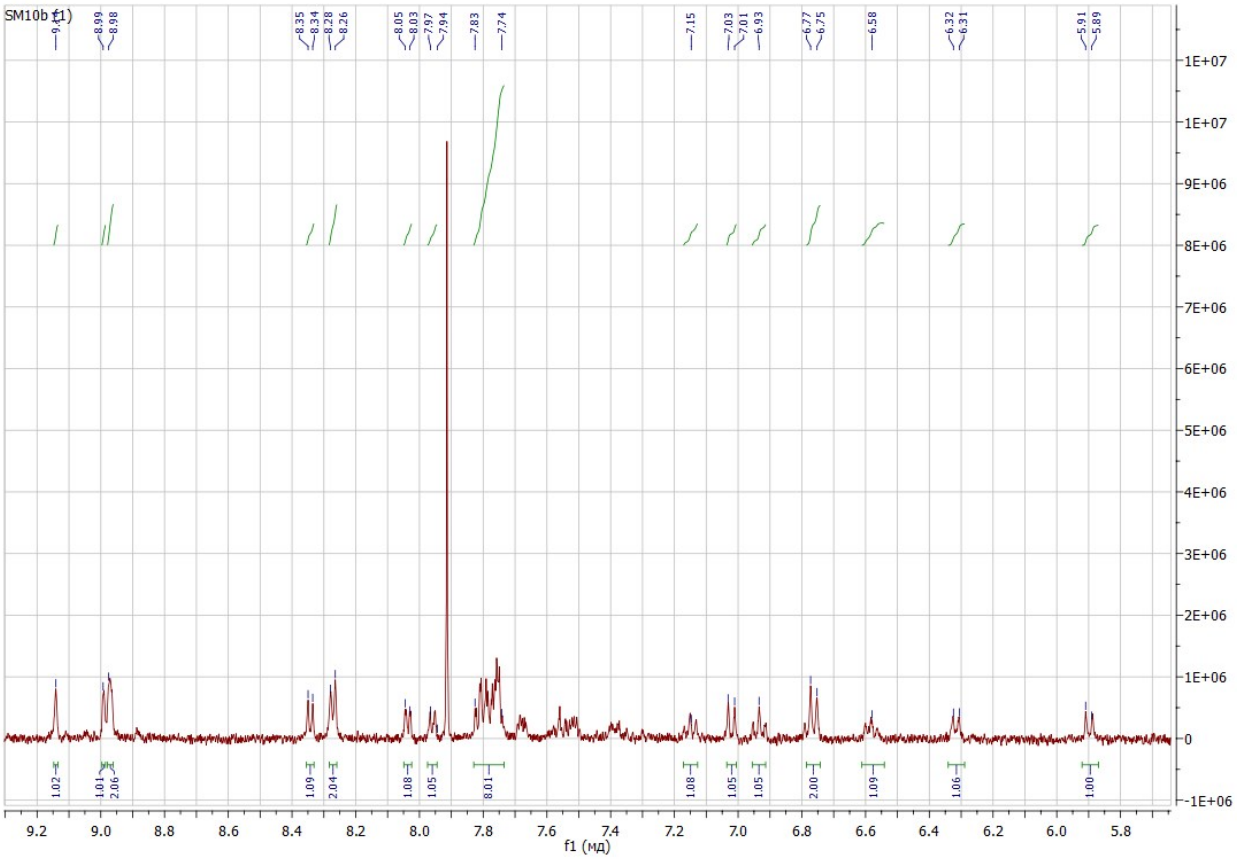

Figure S24. ^{1}H NMR spectrum of **3** after hydrolysis (400 MHz, 298K, CD_3OD).

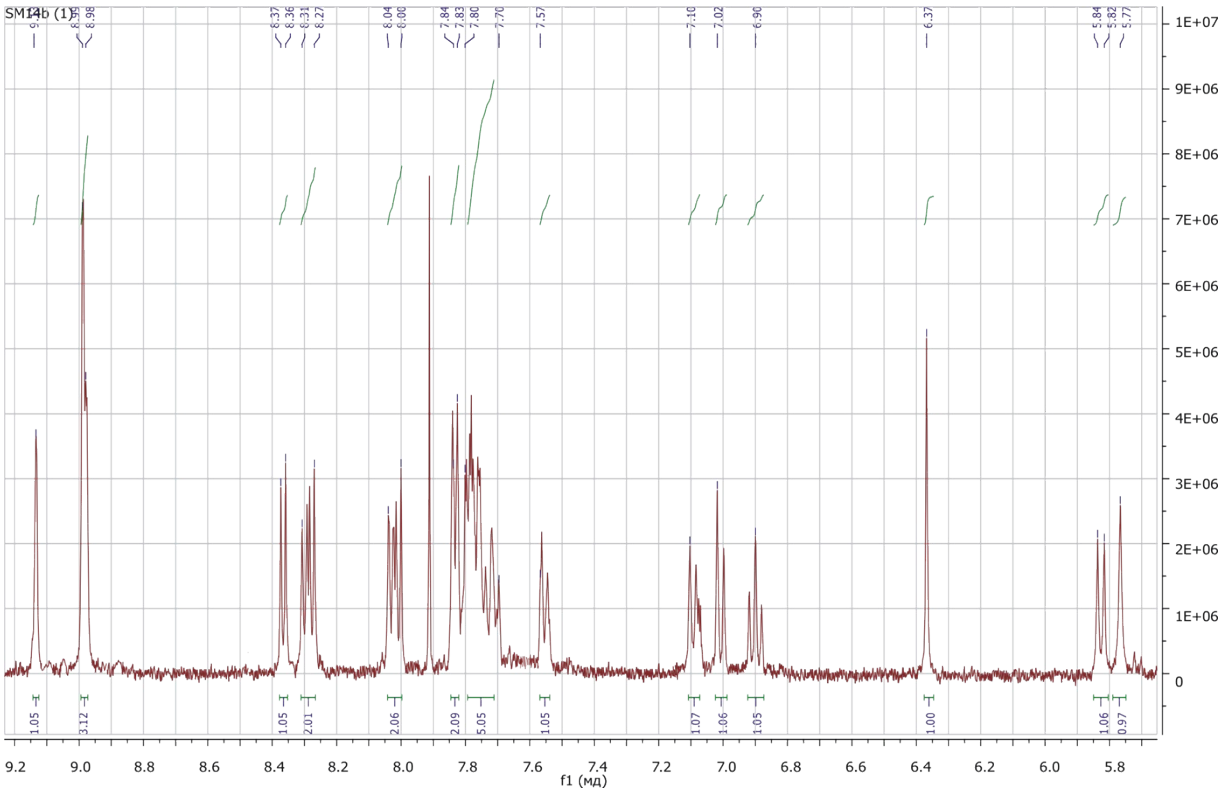

Figure S25. ^{1}H NMR spectrum of **4** after hydrolysis (400 MHz, 298K, CD_3OD).

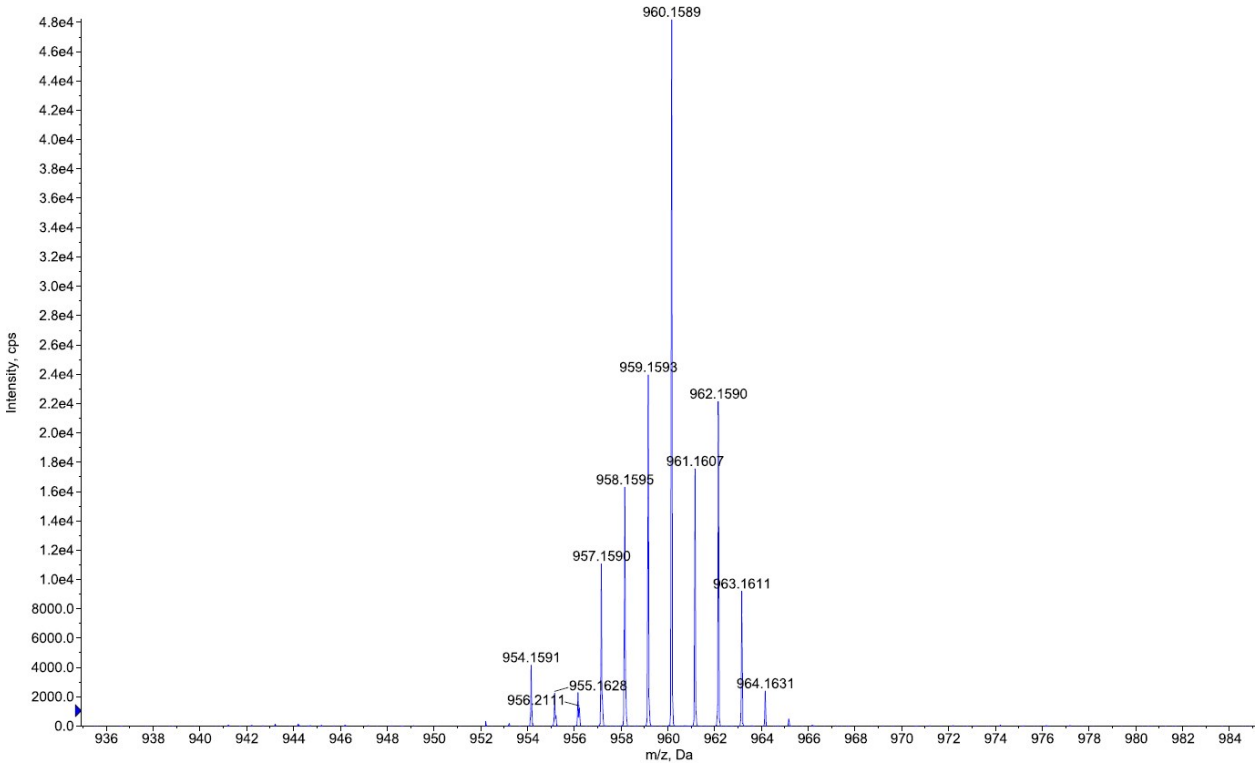

Figure S26. Experimental high resolution mass spectrum of **1**.

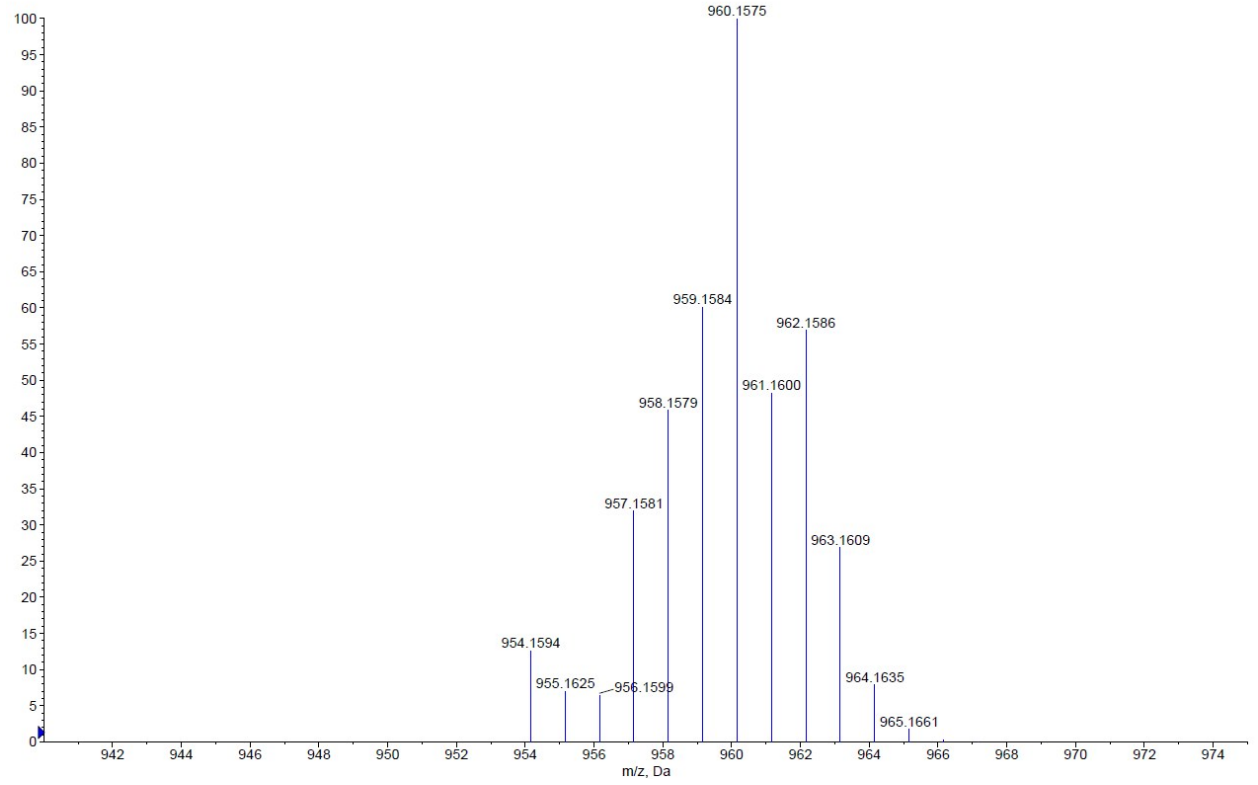

Figure S27. Theoretical high resolution mass spectrum of **1**.

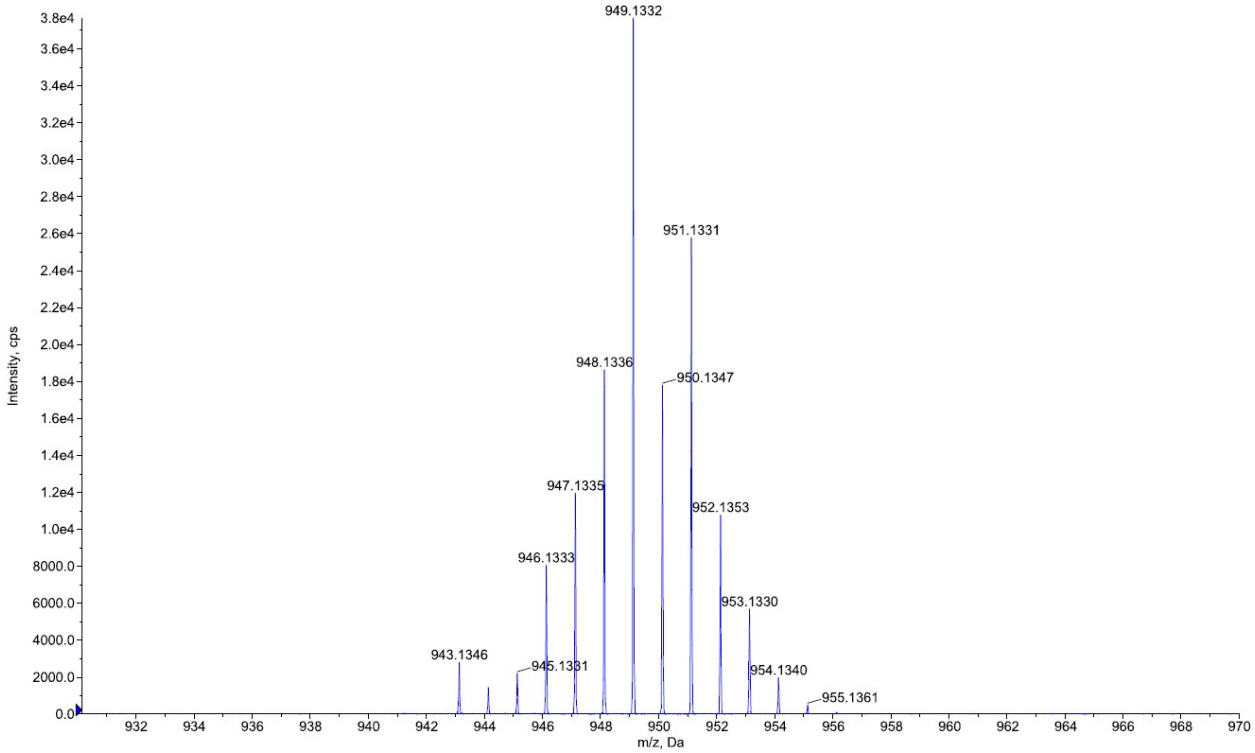

Figure S28. Experimental high resolution mass spectrum of **2**.

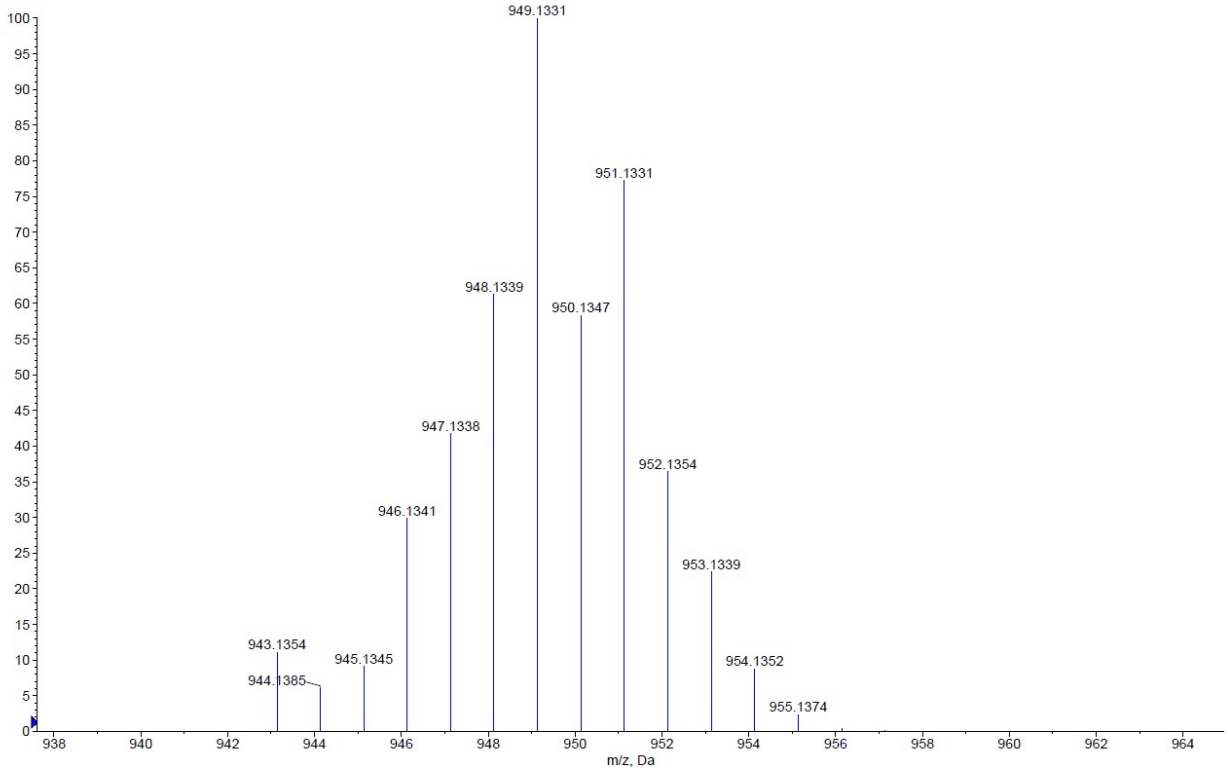

Figure S29. Theoretical high resolution mass spectrum of **2**.

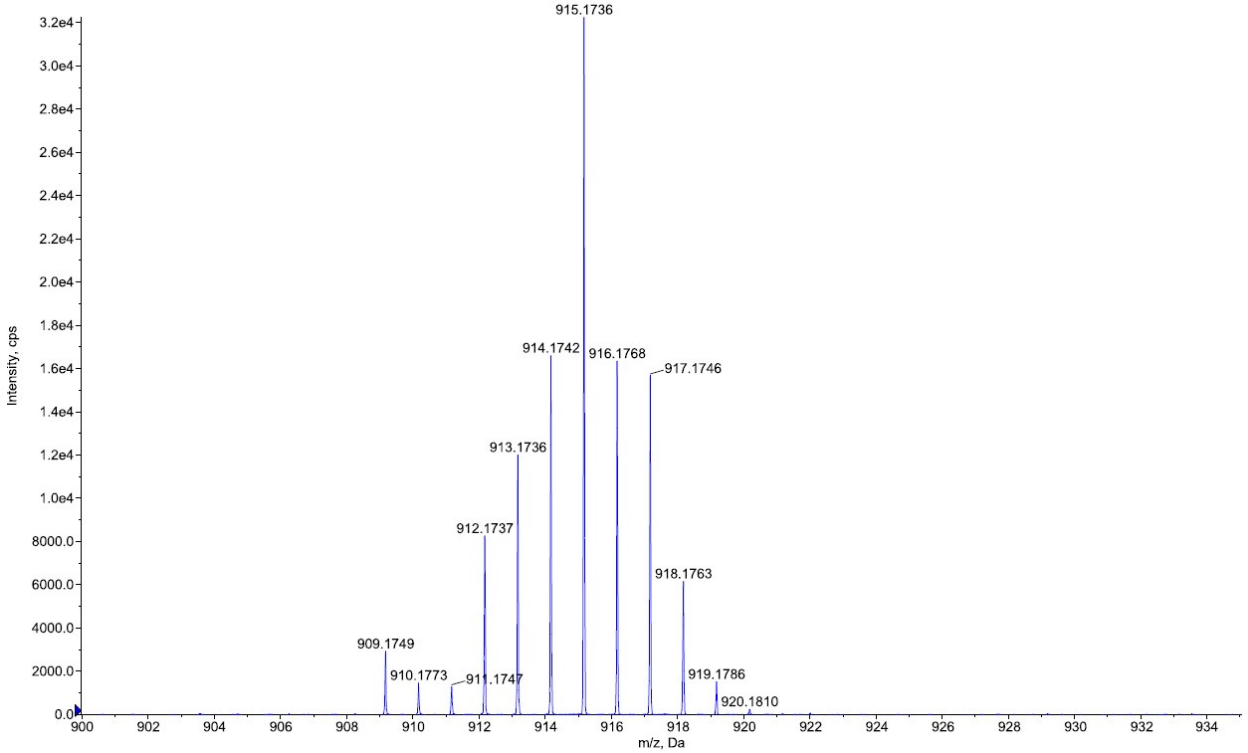

Figure S30. Experimental high resolution mass spectrum of **3**.

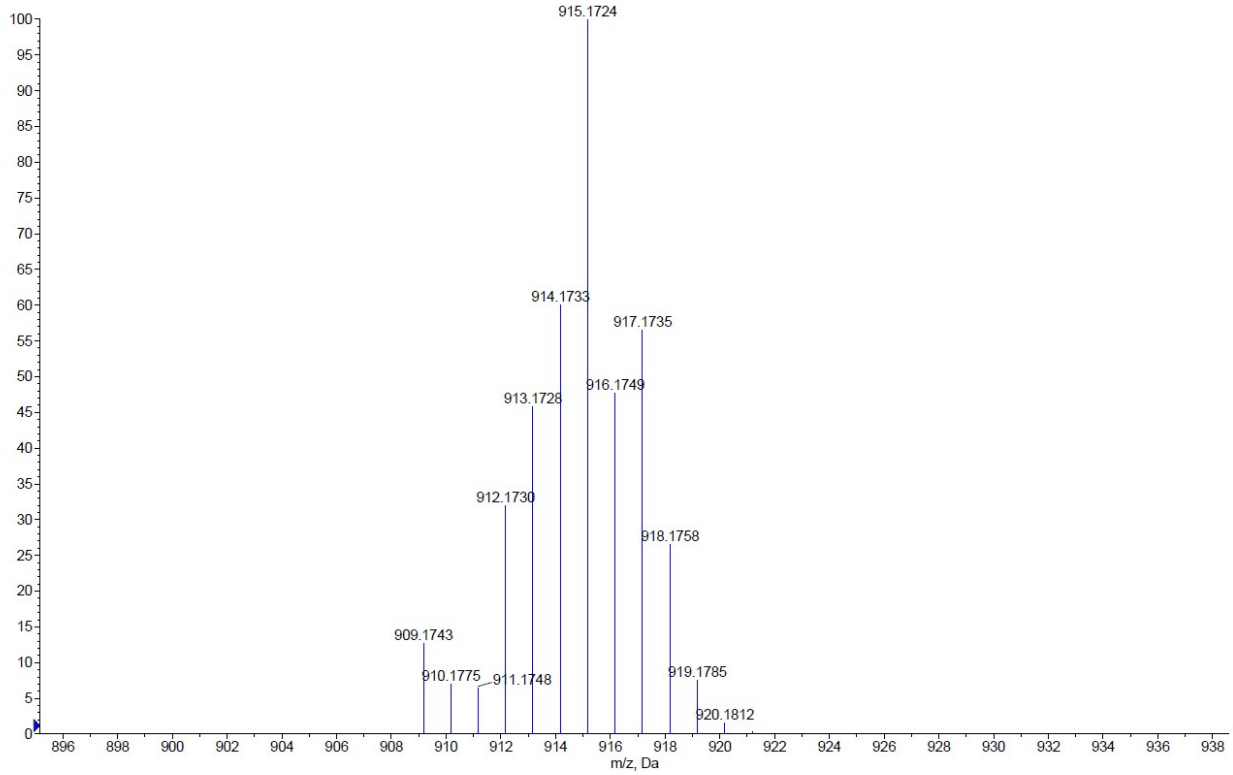

Figure S31. Theoretical high resolution mass spectrum of **3**.

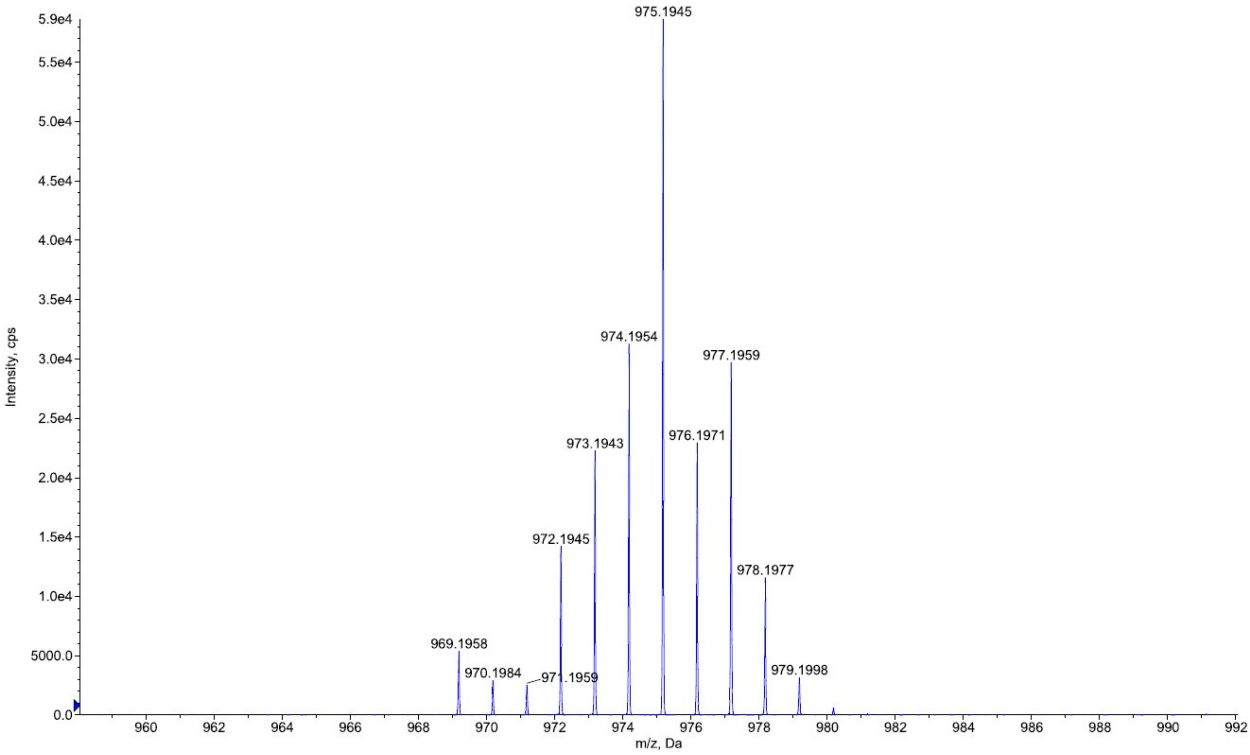

Figure S32. Experimental high resolution mass spectrum of **4**.

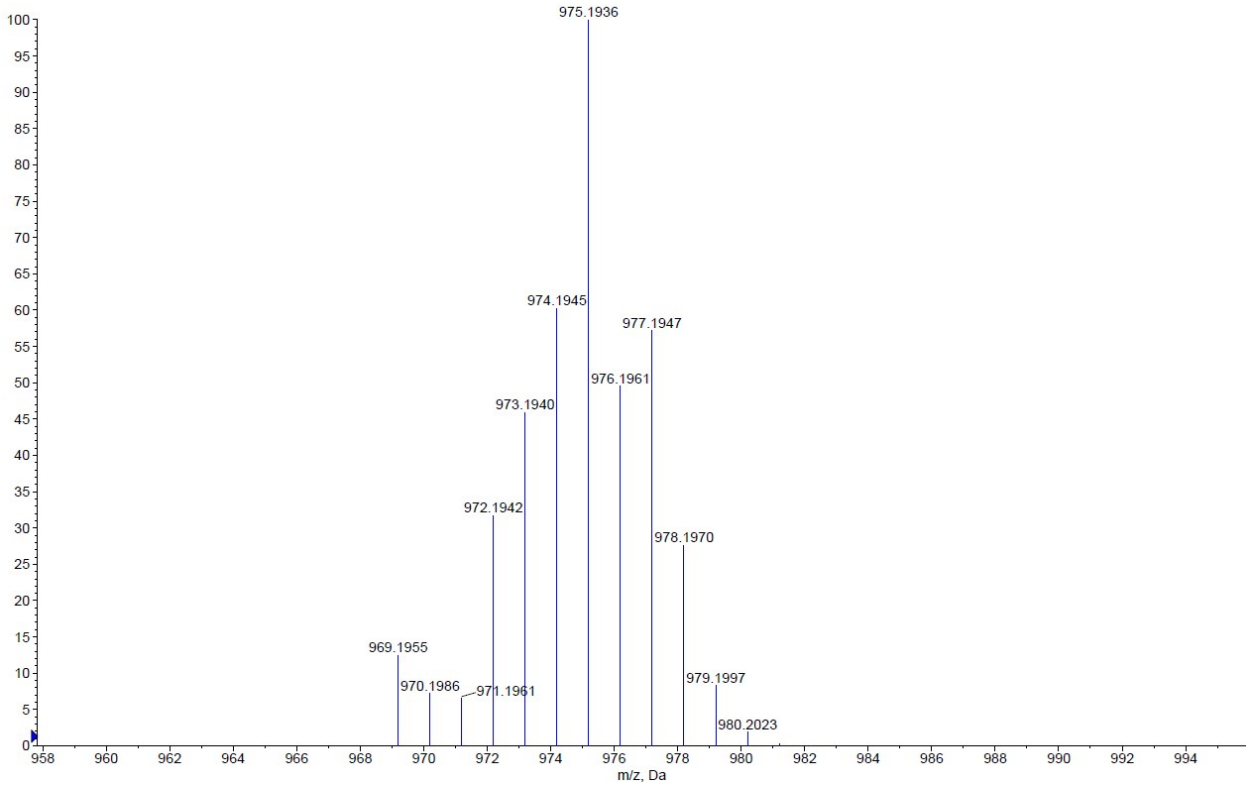

Figure S33. Theoretical high resolution mass spectrum of **4**.

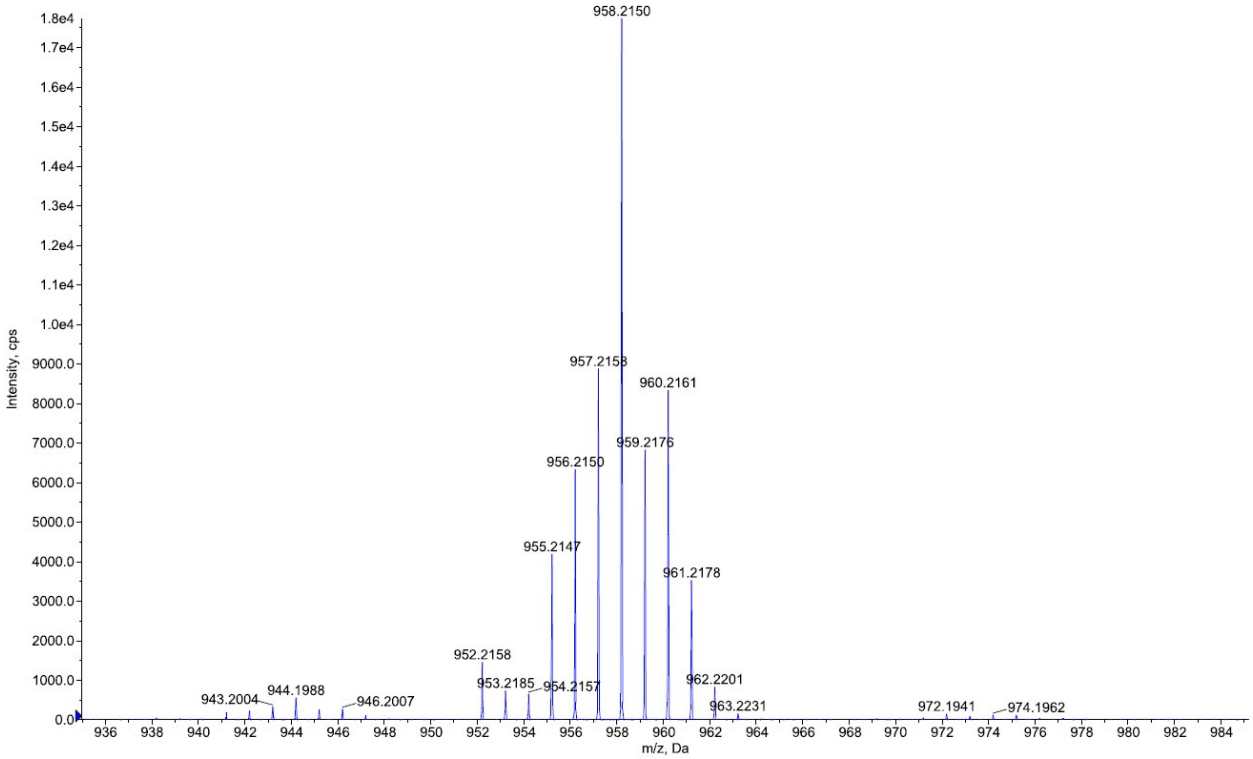

Figure S34. Experimental high resolution mass spectrum of **5**.

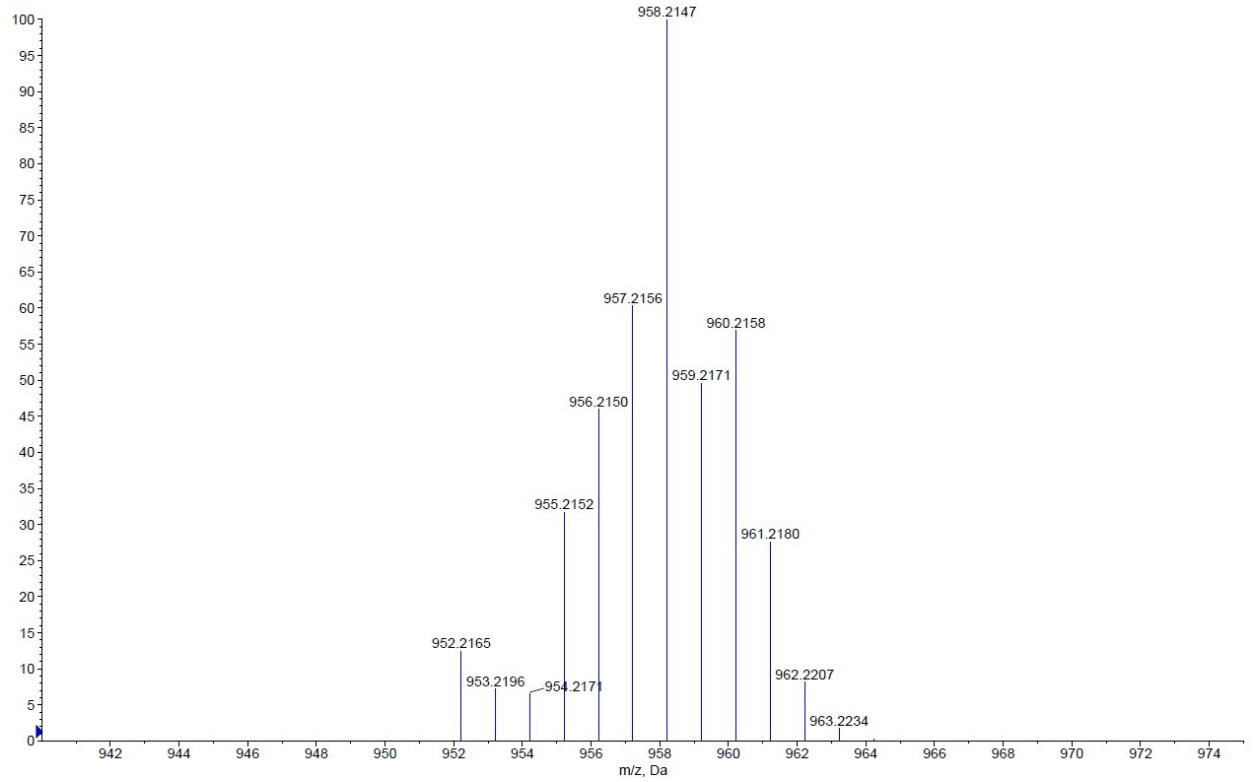

Figure S35. Theoretical high resolution mass spectrum of **5**.

3. **X-ray data**

Table S1. Details of the X-ray data collection and structure refinement for [Ru(η^6-*p*-cymene)(κ^2-*C*,*N*-pbi-NO_2)(*N*,C-pbi-NO_2)] and complexes **3** and **5**.

	[Ru(η^6-*p*-cymene)(κ^2-*C*,*N*-pbi-NO_2)(*N*,C-pbi-NO_2)][PF_6]	**3**	**5**
Empirical formula	$[C_{48}H_{39}N_6O_4Ru][PF_6]\cdot 3CHCl_3$	$1.5[C_{47}H_{37}N_6O_8Ru][PF_6]\cdot CH_2Cl_2$	$[C_{49}H_{42}N_7O_8Ru][PF_6]\cdot CH_2Cl_2$
M_w	1367.99	1674.72	1187.86
Temperature (K)	150(2)	150(2)	150(2)
Size (mm)	0.21 x 0.07 x 0.04	0.18 x 0.15 x 0.08	0.33 x 0.23 x 0.2
Cryst. system	triclinic	monoclinic	triclinic
Space group	P-1	C2/c	P-1
a (Å)	16.4300(7)	53.215(3)	11.3865(4)
b (Å)	17.9246(9)	12.7933(6)	14.9295(5)
c (Å)	19.3808(7)	21.3714(9)	18.3394(6)
α (°)	83.218(2)		77.5950(10)
β (°)	85.892(2)	102.3941(15)	84.1060(10)
γ (°)	79.659(2)		77.8560(10)
V (Å^3)	5568.2(4)	14210.4(11)	2971.28(17)
Z	4	8	2
ρ_{cald} (g·cm^{-3})	1.632	1.566	1.328
Abs coeff (mm^{-1})	0.813	0.525	0.452
F(000)	2752	6792	1208
θ range (deg)	$1.86 < \theta < 25.03$	$1.64 < \theta < 24.50$	$1.83 < \theta < 30.70$
no. of collected/unique rflns	53144 / 19298	55769 / 11798	36788 / 18004
Completeness to *θ* (%)	98.1	99.8	97.6
no. of data/restraints/params	19298 / 17 / 1413	11798 / 2 / 951	18004 / 0 / 682
Goodness of fit on F^2	0.983	1.191	1.029
Final *R* indices ($I > 2\sigma(I)$)	R1 = 0.0841, wR2 = 0.1862	R1 = 0.0735 / wR2 = 0.1573	R1 = 0.0613, wR2 = 0.1412
R indices (all data)	R1 = 0.1621, wR2 = 0.2179	R1 = 0.0811 / wR2 = 0.1610	R1 = 0.0812, wR2 = 0.1510
Largest diff peak/hole (e/Å^3)	1.55 / −1.46	1.08 / −1.44	1.87 / −0.80

Table S2. Selected distances [Å] and angles [°] in structures of [Ru(η^6-*p*-cymene)(κ^2-*C*,*N*-pbi-NO_2)(*N*,C-pbi-NO_2)][PF_6] and complexes **3** and **5**.

[Ru(η^6-*p*-cymene)(κ^2-*C*,*N*-pbi-NO_2)(*N*,C-pbi-NO_2)]	Ru_1–C_1	Ru_1–N_1	Ru_1–N_2	Ru_1–η^6-*p*-cymene (centroid)			
	2.089(7)	2.090(7)	2.163(7)	1.725(8)			
	C_1–Ru_1–centroid		N_1–Ru_1–centroid		N_2–Ru_1–centroid		
	127.2(3)		129.1(3)		130.8(2)		
Complex **3**	Ru_1–C_1	Ru_1–N_1	Ru_1–N_3	Ru_1–N_4	Ru_1–N_5	Ru_1–N_6	
	2.075(6)	2.074(5)	2.051(4)	2.127(4)	2.019(4)	2.017(4)	
	C_1–Ru_1–N_3	C_1–Ru_1–N_5	C_1–Ru_1–N_6	N_1–Ru_1–N_3	N_1–Ru_1–N_4	N_1–Ru_1–N_6	N_4–Ru_1–N_5
	95.53(18)	93.4(2)	88.89(19)	86.46(17)	97.97(17)	97.75(17)	90.46(16)
Complex **5**	Ru_1–C_1	Ru_1–N_1	Ru_1–N_3	Ru_1–N_4	Ru_1–N_5	Ru_1–N_6	
	2.061(3)	2.105(2)	2.056(2)	2.124(2)	2.029(2)	2.015(2)	
	C_1–Ru_1–N_3	C_1–Ru_1–N_5	C_1–Ru_1–N_6	N_1–Ru_1–N_3	N_1–Ru_1–N_4	N_1–Ru_1–N_6	N_4–Ru_1–N_5
	95.88(10)	90.68(10)	90.14(10)	88.73(9)	93.20(9)	94.96(9)	97.28(9)

4. Optical properties.

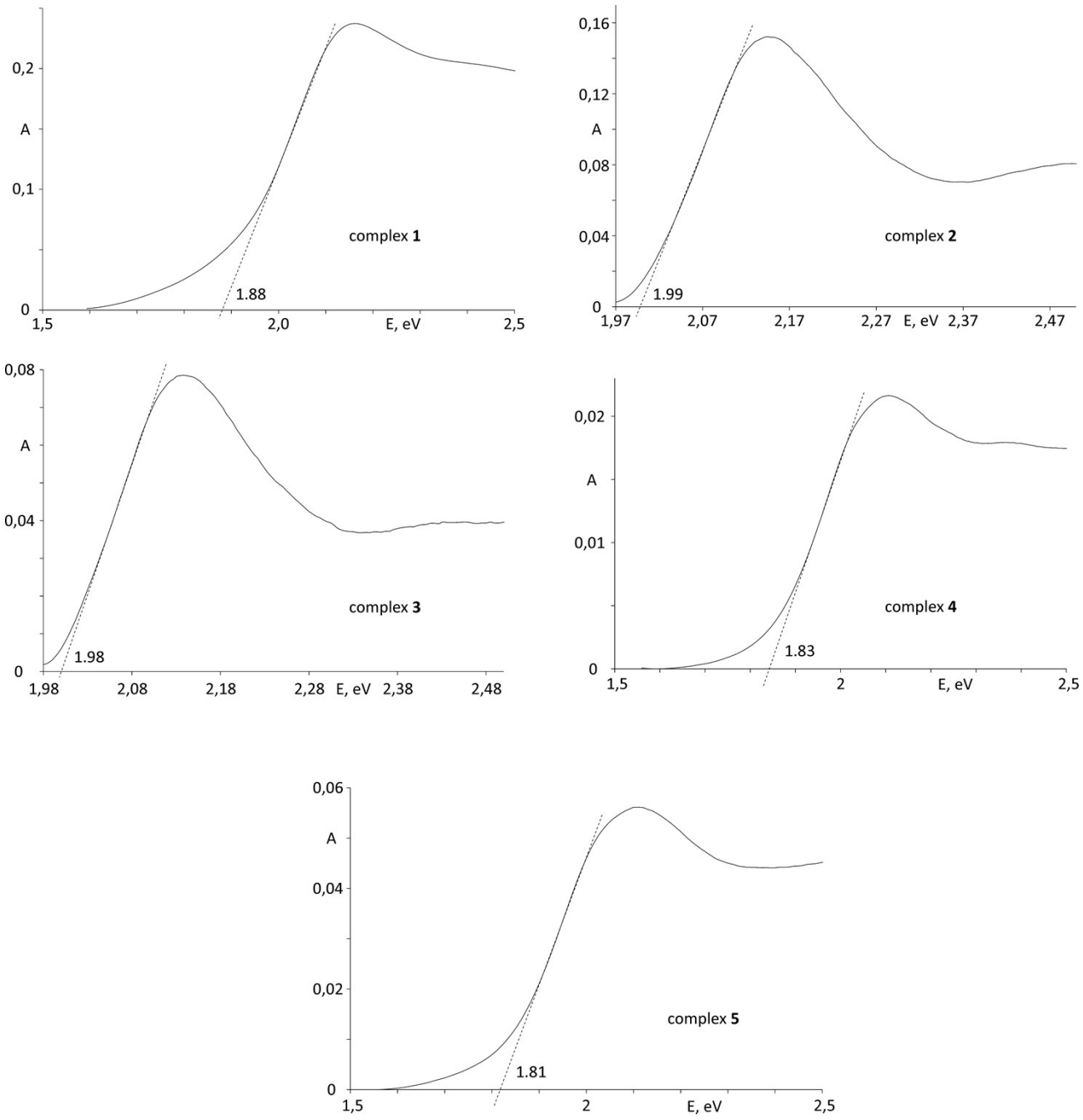

Figure S36. Diffuse reflectance spectra of **1** – **5**.

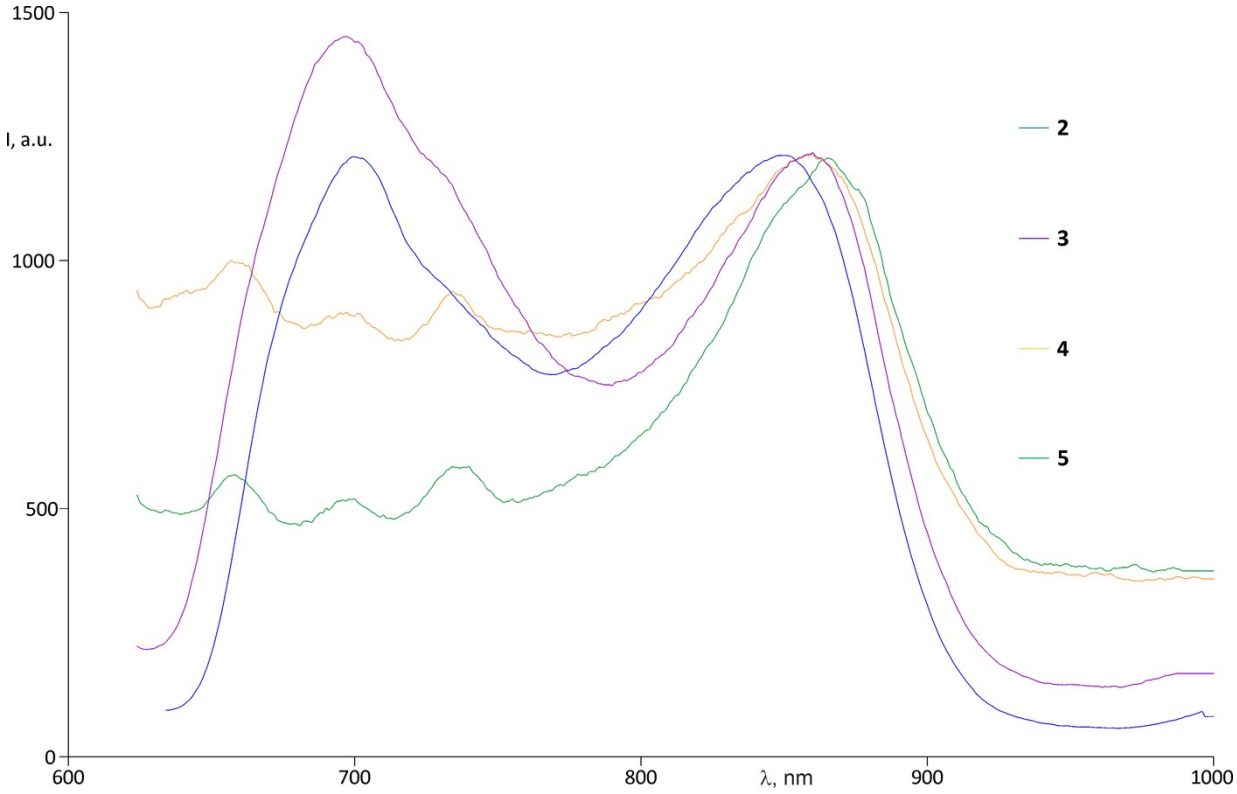

Figure S37. Luminescence spectra of **1** – **5**.

5. Calculation details.

Table S3. Frontier molecular orbitals energy and composition for complexes **1** – **5**.

complex	moiety	**1**	**2**	**3**	**4**	**5**
HOMO-4	Ru	10	11	12	16	1
	C^N	54	53	52	51	63
	N^N	36	36	36	33	36
	energy, eV	-9.08	-8.91	-8.87	-8.56	-8.61
HOMO-3	Ru	14	29	20	63	76
	C^N	55	50	51	30	17
	N^N	31	21	29	7	7
	energy, eV	-8.70	-8.31	-8.37	-7.92	-7.78
HOMO-2	Ru	76	75	76	69	76
	C^N	10	7	7	8	10
	N^N	14	18	17	23	14
	energy, eV	-8.05	-7.91	-7.84	-7.72	-7.72
HOMO-1	Ru	77	67	70	57	54
	C^N	12	18	18	25	20
	N^N	10	15	11	18	26
	energy, eV	-8.02	-7.87	-7.82	-7.65	-7.54
HOMO	Ru	62	55	56	26	9
	C^N	20	29	26	56	70
	N^N	18	16	18	18	21
	energy, eV	-7.80	-7.64	-7.55	-7.11	-7.03
LUMO	Ru	7	7	7	8	7
	C^N	4	3	3	3	4
	N^N	89	90	90	89	89
	energy, eV	-5.20	-5.11	-5.05	-4.97	-4.97
LUMO+1	Ru	13	14	14	14	16
	C^N	4	3	3	3	3
	N^N	83	83	83	83	81
	energy, eV	-5.03	-4.95	-4.91	-4.80	-4.82
LUMO+2	Ru	2	3	3	3	3
	C^N	12	1	1	1	1
	N^N	86	96	96	96	96
	energy, eV	-4.53	-4.43	-4.38	-4.30	-4.29

Table S4. TDDFT singlet excited states for **1** – **5**.

Complex	State	λ / nm (f)	Dominant monoexcitations
1	S1	693 (0,004)	H → L (90%)
	S4	589 (0,035)	H-1 → L (18%) H-2 → L (18%) H-1 → L+1 (24%) H-2 → L+1 (37%)
	S5	547 (0,167)	H-2 → L (55%) H-1 → L+1 (35%)
2	S1	708 (0,003)	H → L (92%)
	S2	607 (0,058)	H-1 → L (44%) H-1 → L+1 (36%)
	S3	556 (0,171)	H-1 → L (56%) H-1 → L+1 (25%)
3	S1	722 (0,003)	H → L (92%)
	S4	614 (0,055)	H-1 → L (46%) H-1 → L+1 (34%)
	S5	561 (0,175)	H-1 → L (12%) H-1 → L+1 (35%) H-2 → L (35%)
4	S1	826 (0,002)	H → L (93%)
	S4	619 (0,03)	H-1 → L (27%) H-1 → L+1 (33%) H-2 → L+1 (22%)
	S5	582 (0,09)	H-2 → L (35%) H-1 → L+1 (32%)
	S9	532 (0,11)	H-3 → L (53%) H → L+2 (15%) H → L+3 (12%)
5	S1	823 (0,002)	H → L (89%)
	S6	605 (0,04)	H-3 → L+1 (40%) H-3 → L (32%) H-2 → L+1 (12%)
	S7	564 (0,121)	H-3 → L (34%) H-2 → L+1 (31%) H → L+2 (9%)

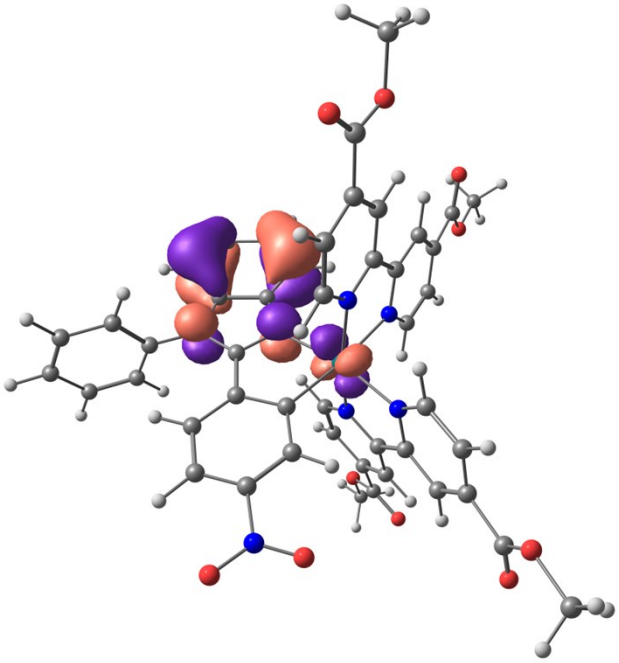

HOMO-4

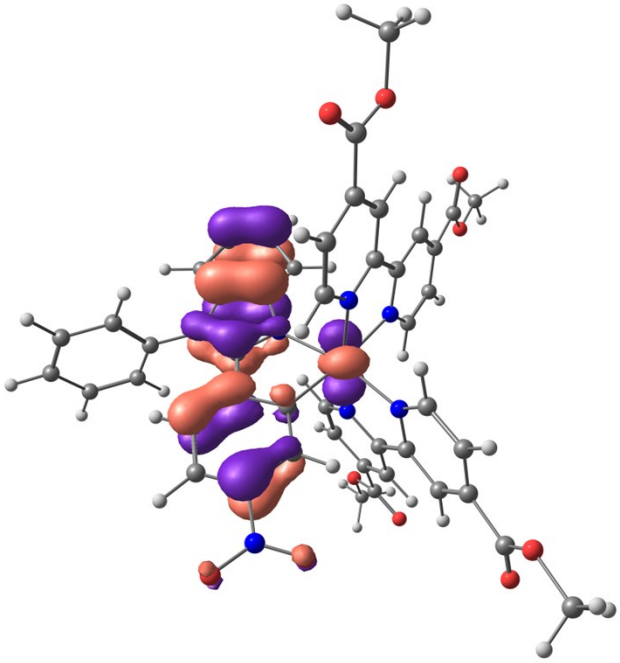

HOMO-3

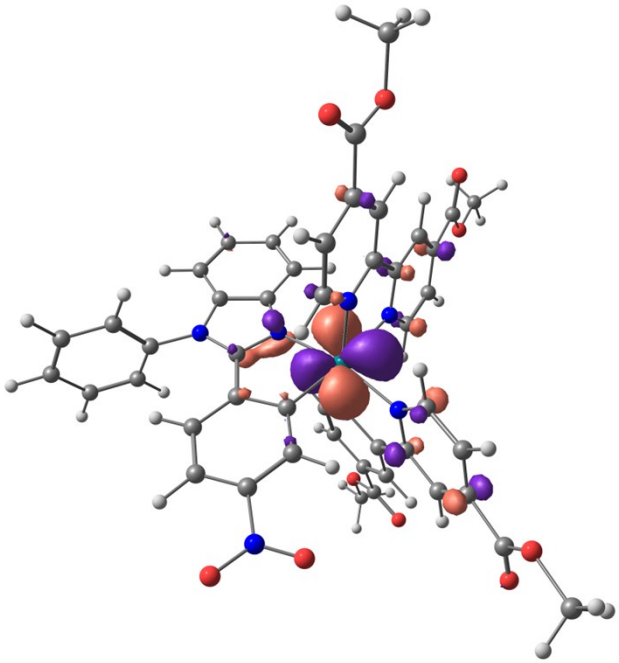

HOMO-2

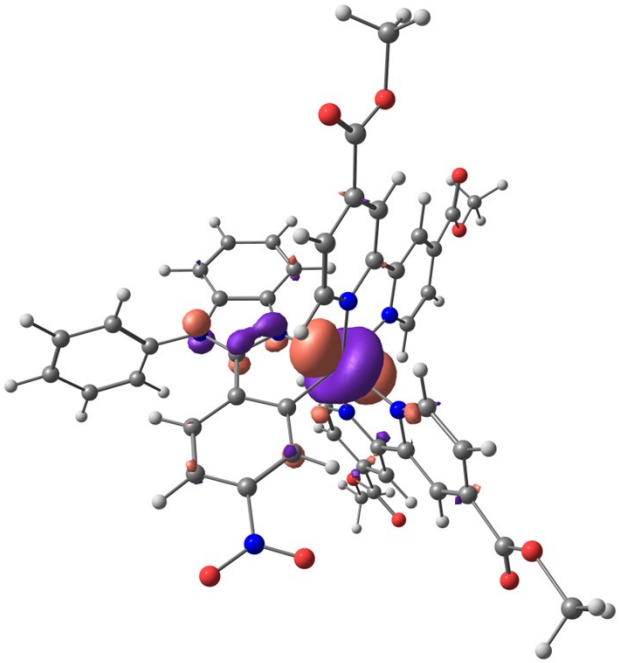

HOMO-1

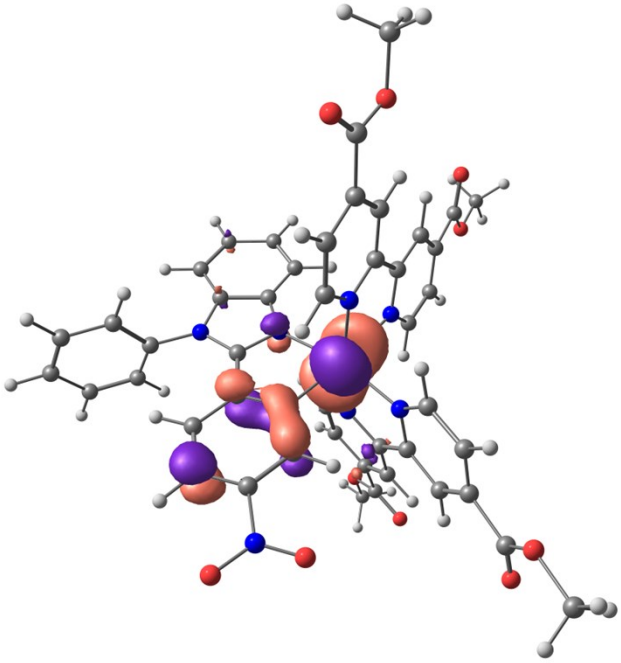

HOMO

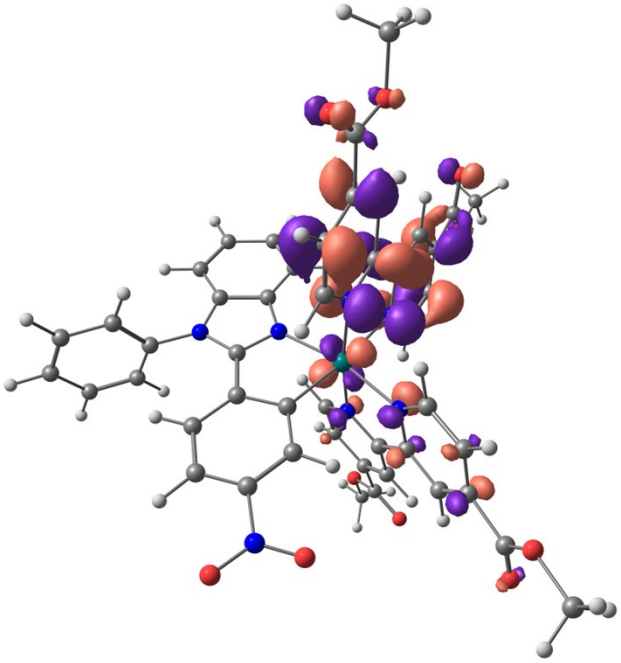

LUMO

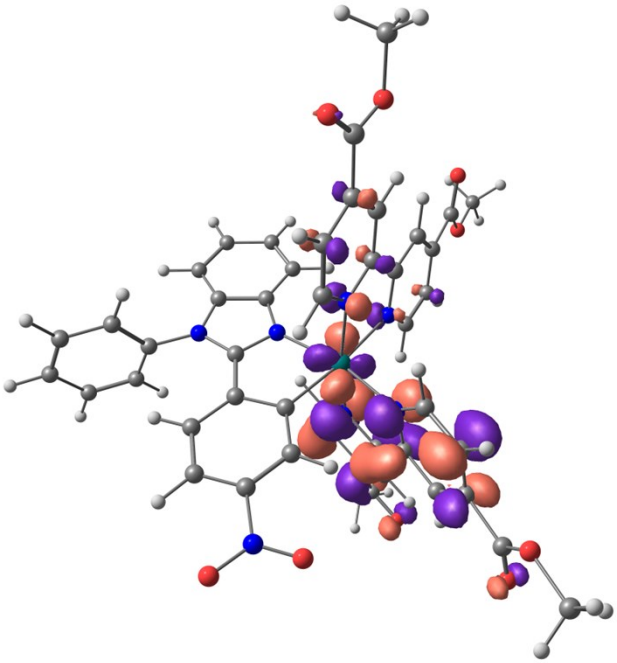

LUMO+1

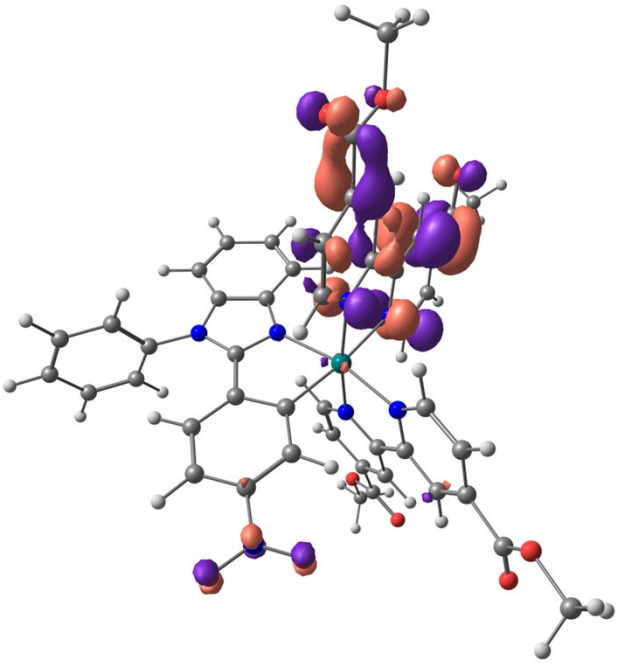

LUMO+2

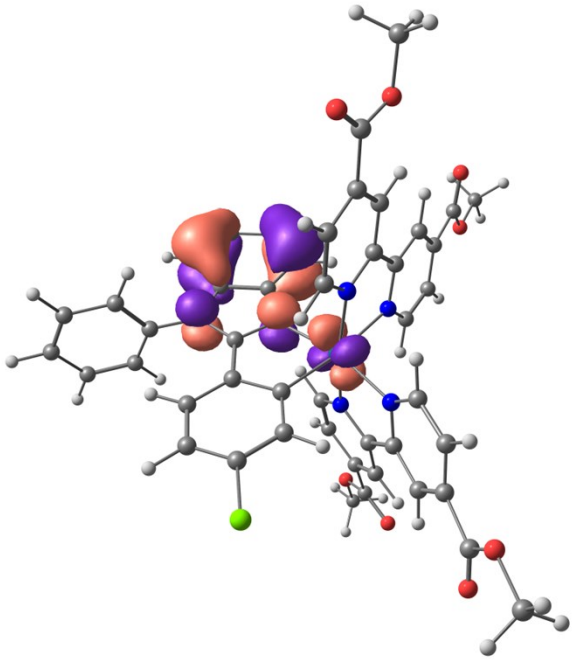

HOMO-4

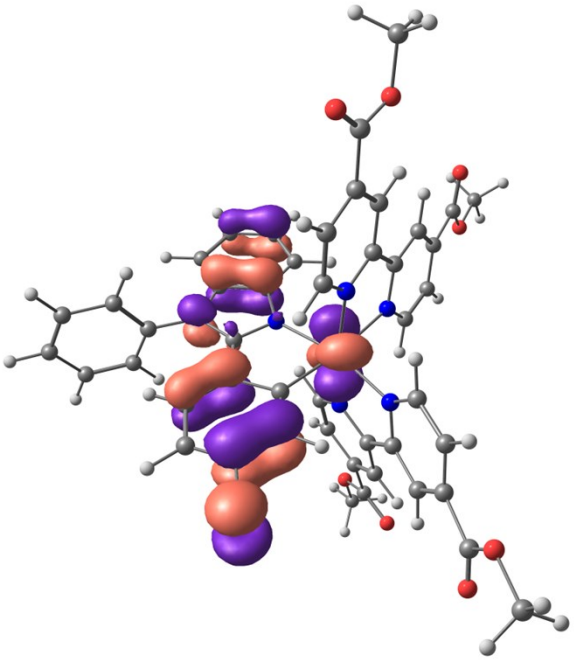

HOMO-3

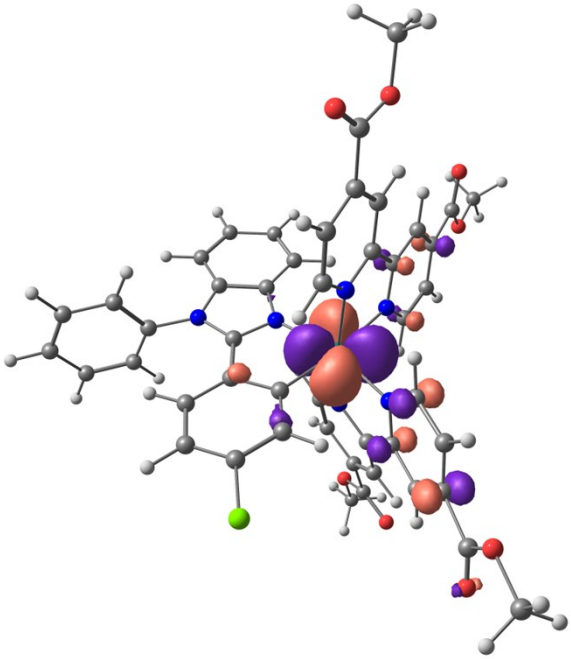

HOMO-2

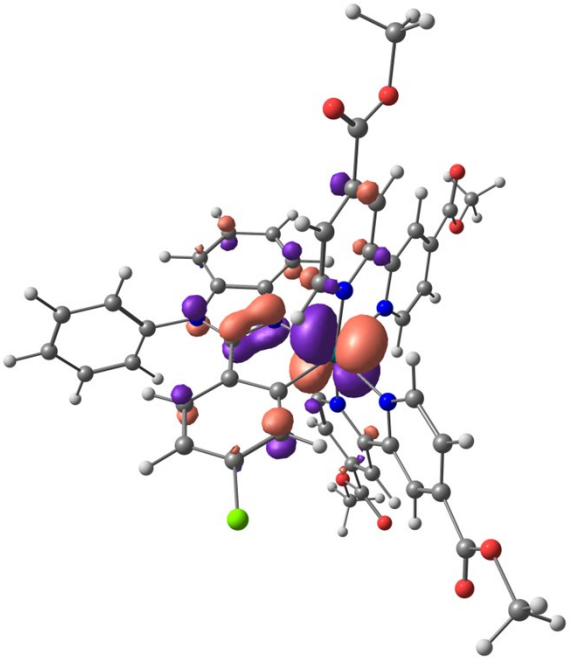

HOMO-1

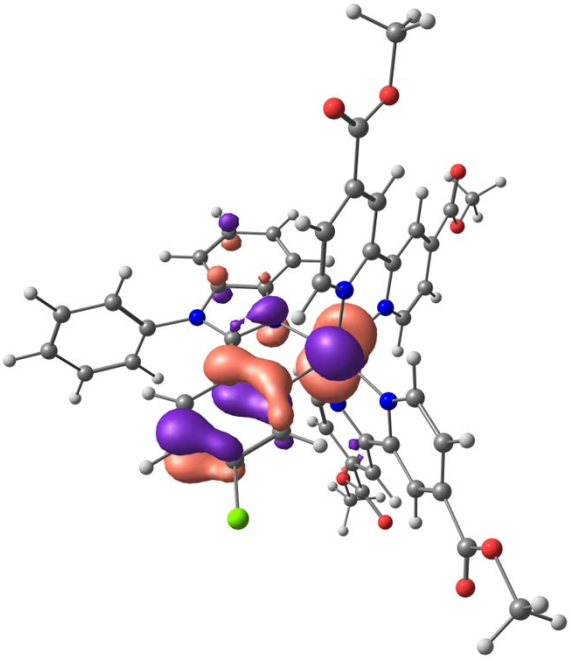

HOMO

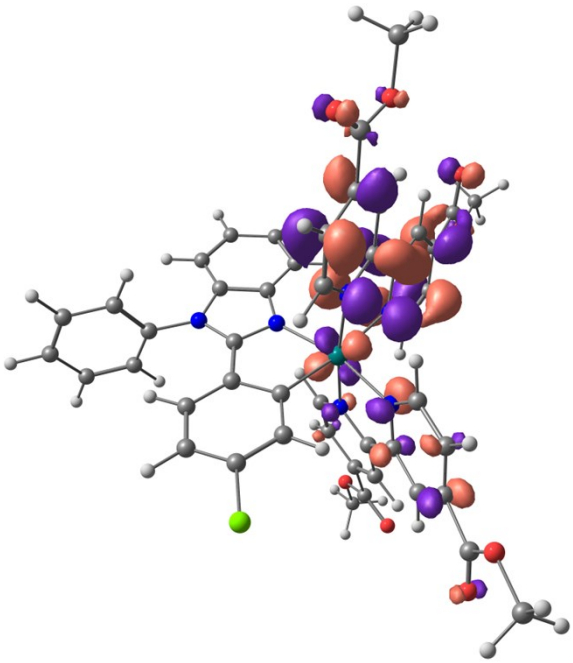

LUMO

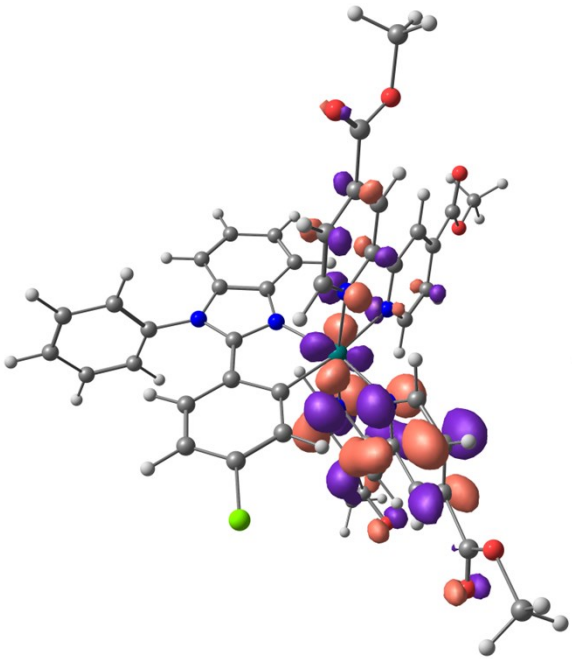

LUMO+1

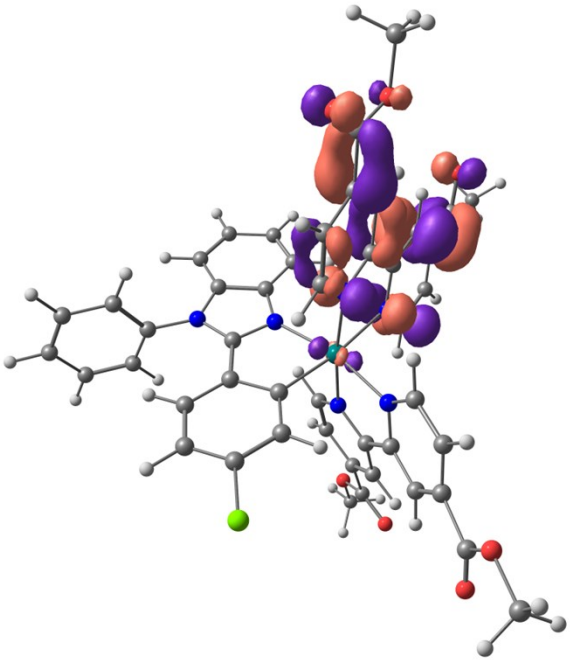

LUMO+2

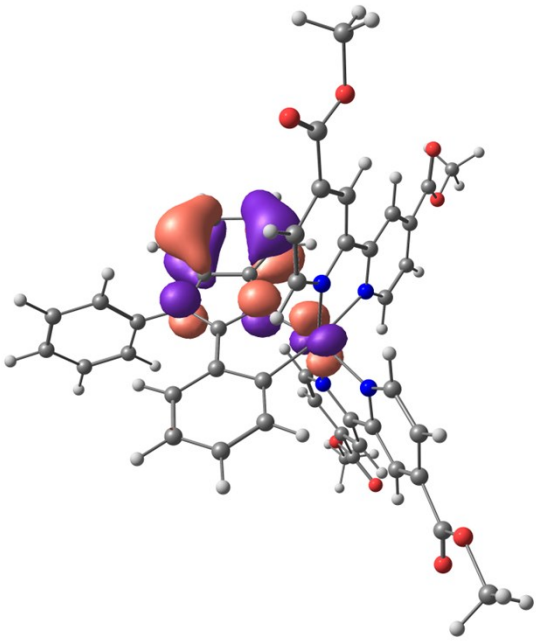

HOMO-4

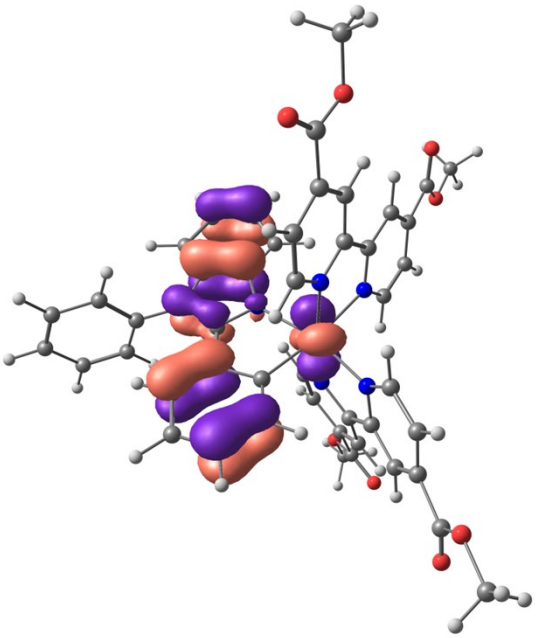

HOMO-3

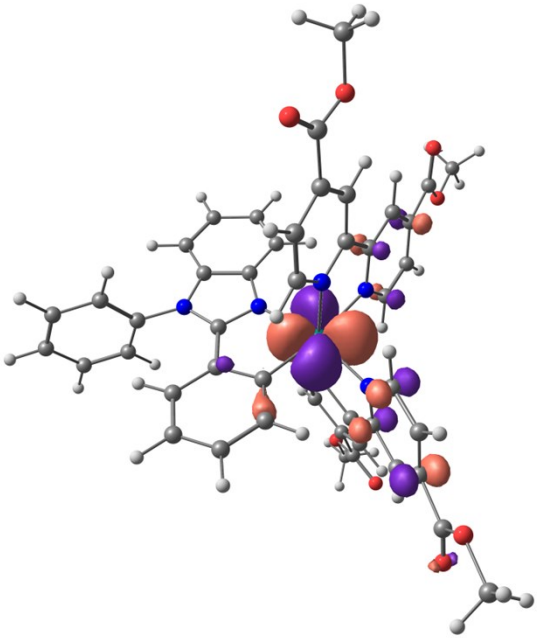

HOMO-2

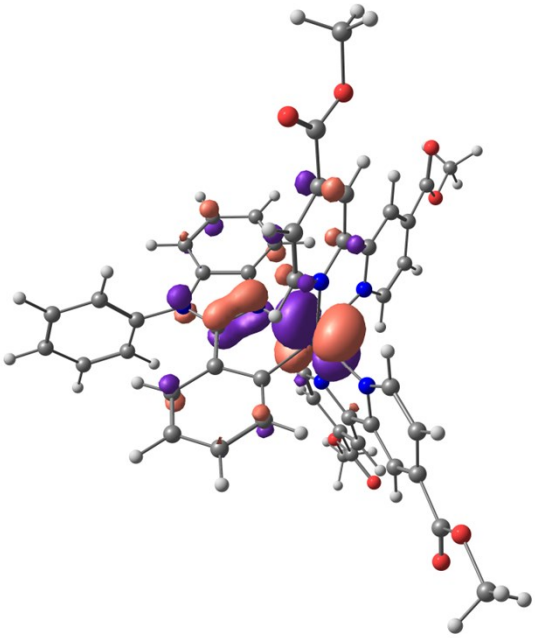

HOMO-1

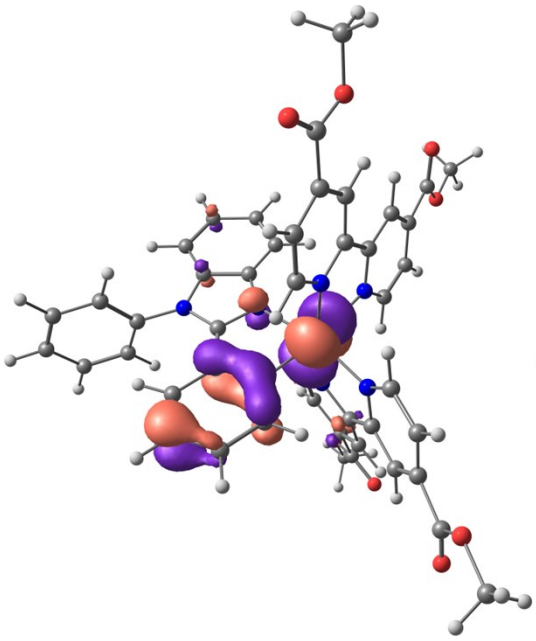

HOMO

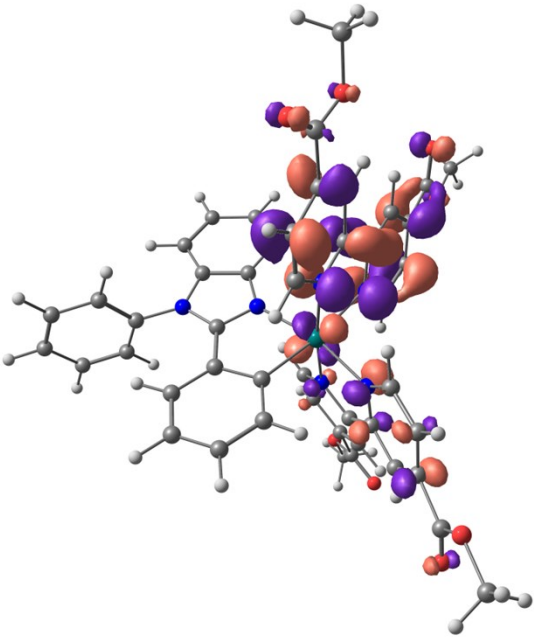

LUMO

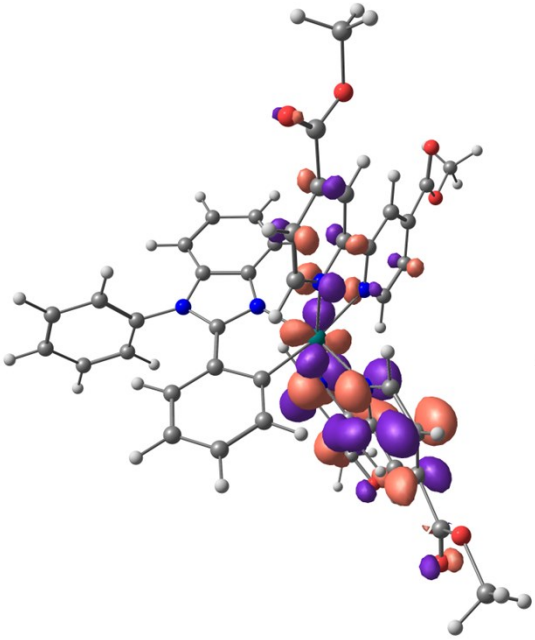

LUMO+1

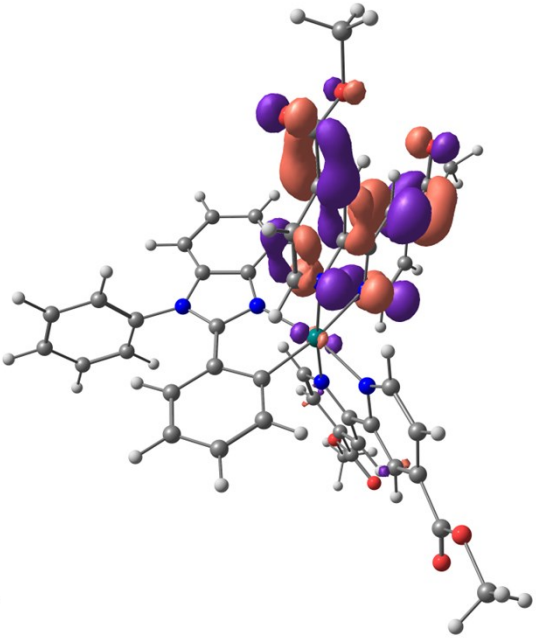

LUMO+2

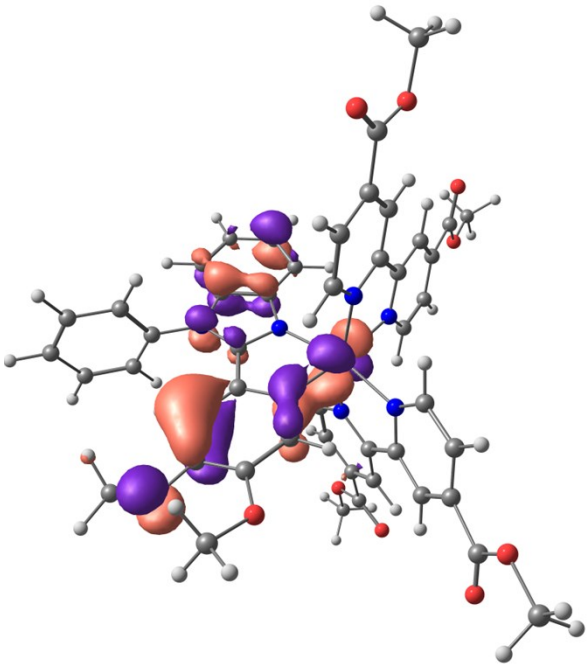

HOMO-4

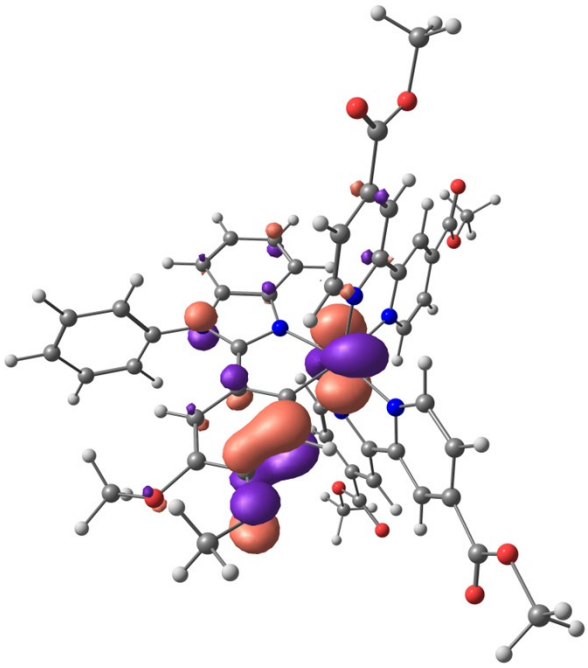

HOMO-3

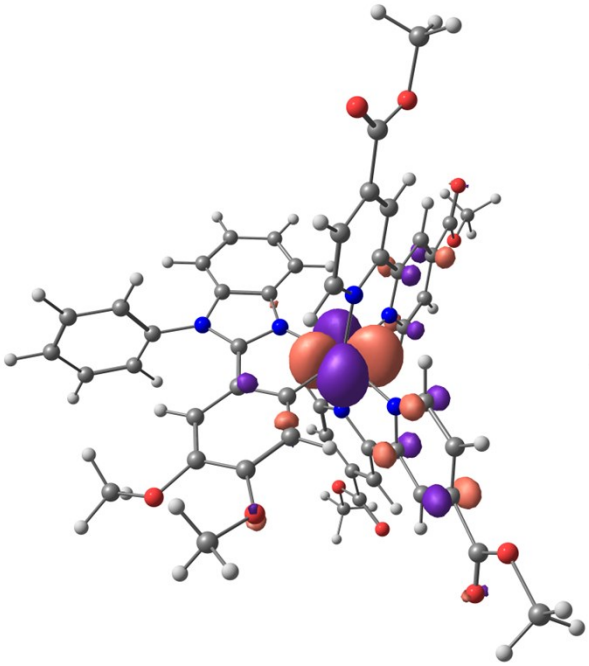

HOMO-2

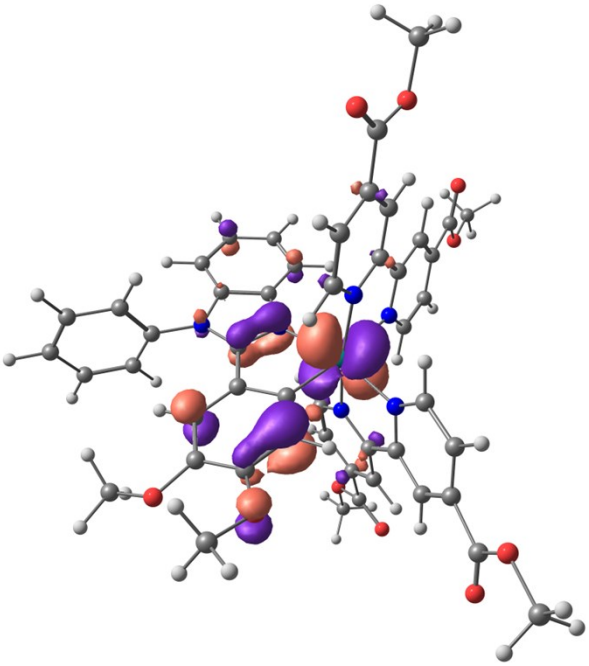

HOMO-1

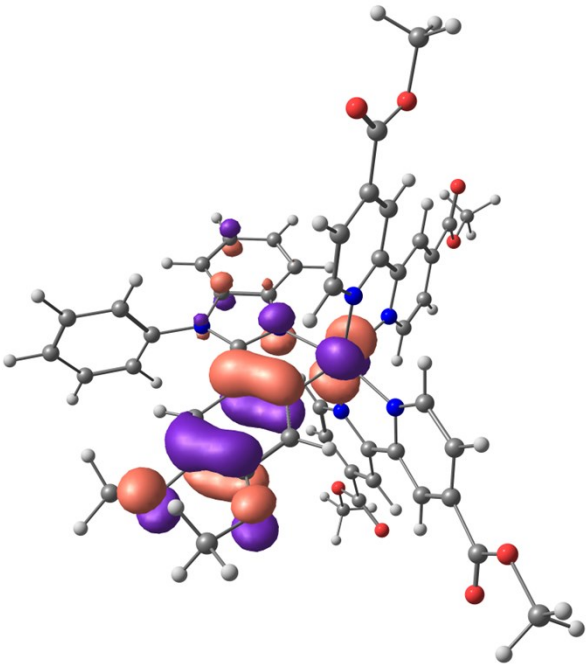

HOMO

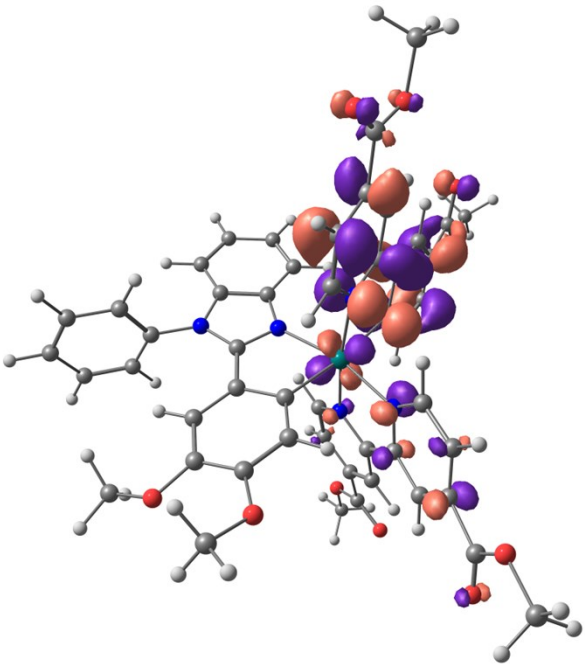

LUMO

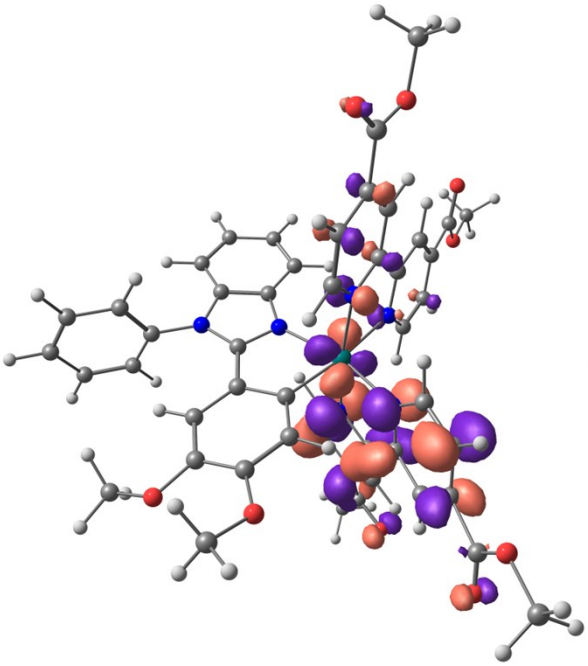

LUMO+1

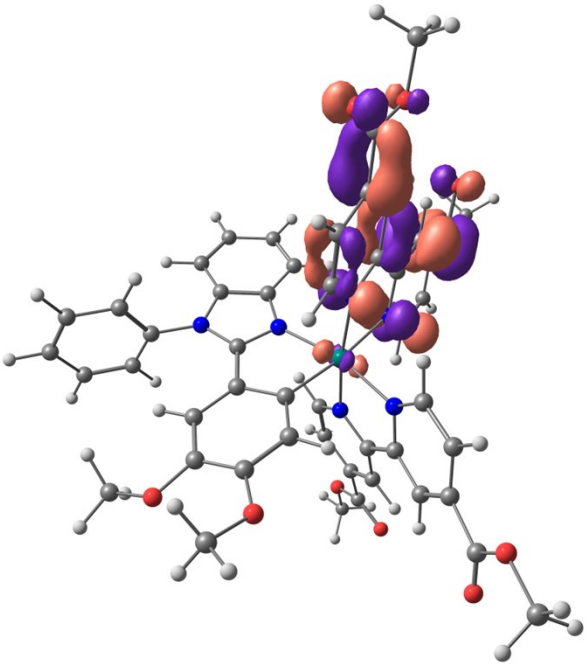

LUMO+2

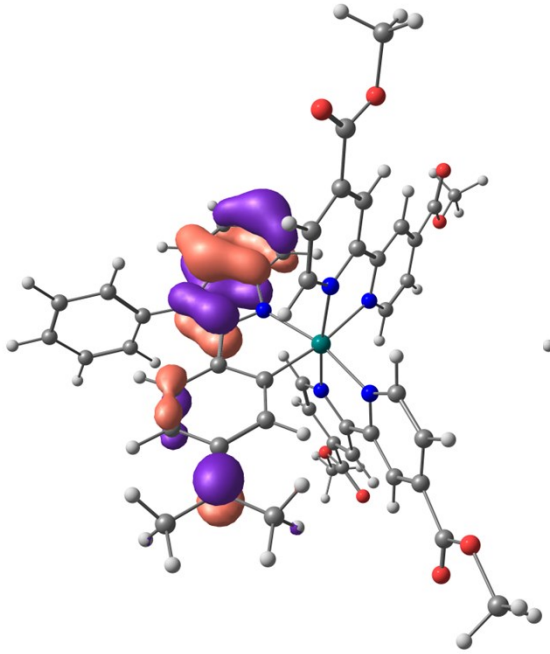

HOMO-4

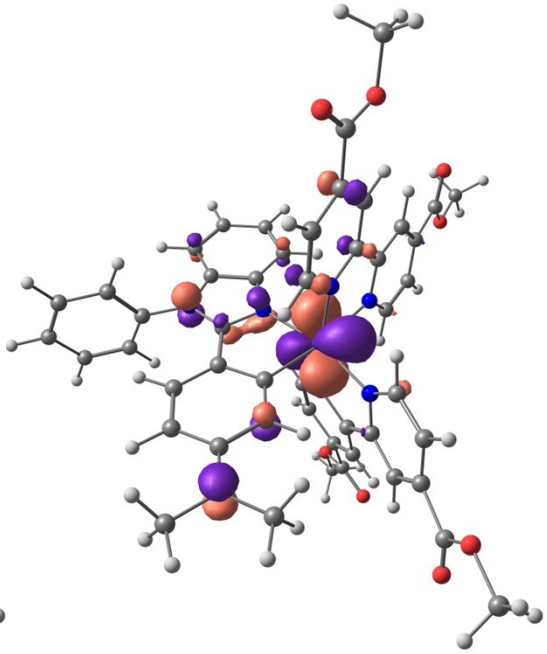

HOMO-3

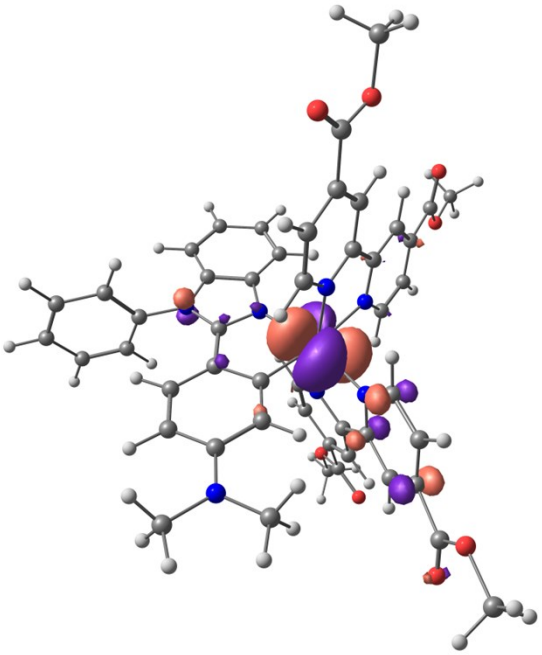

HOMO-2

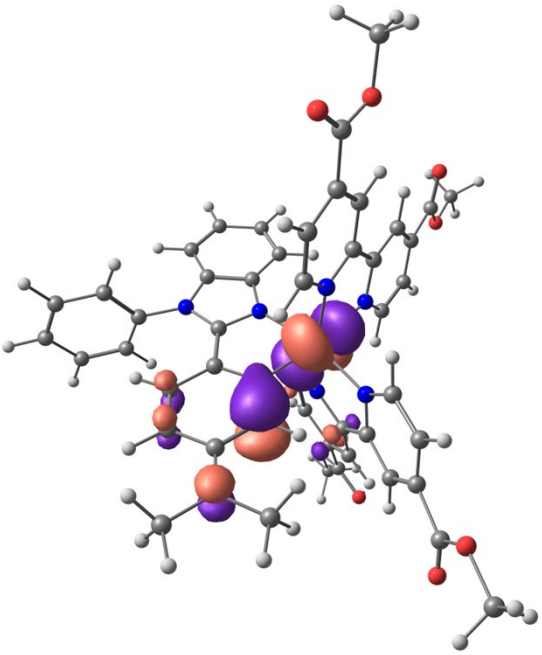

HOMO-1

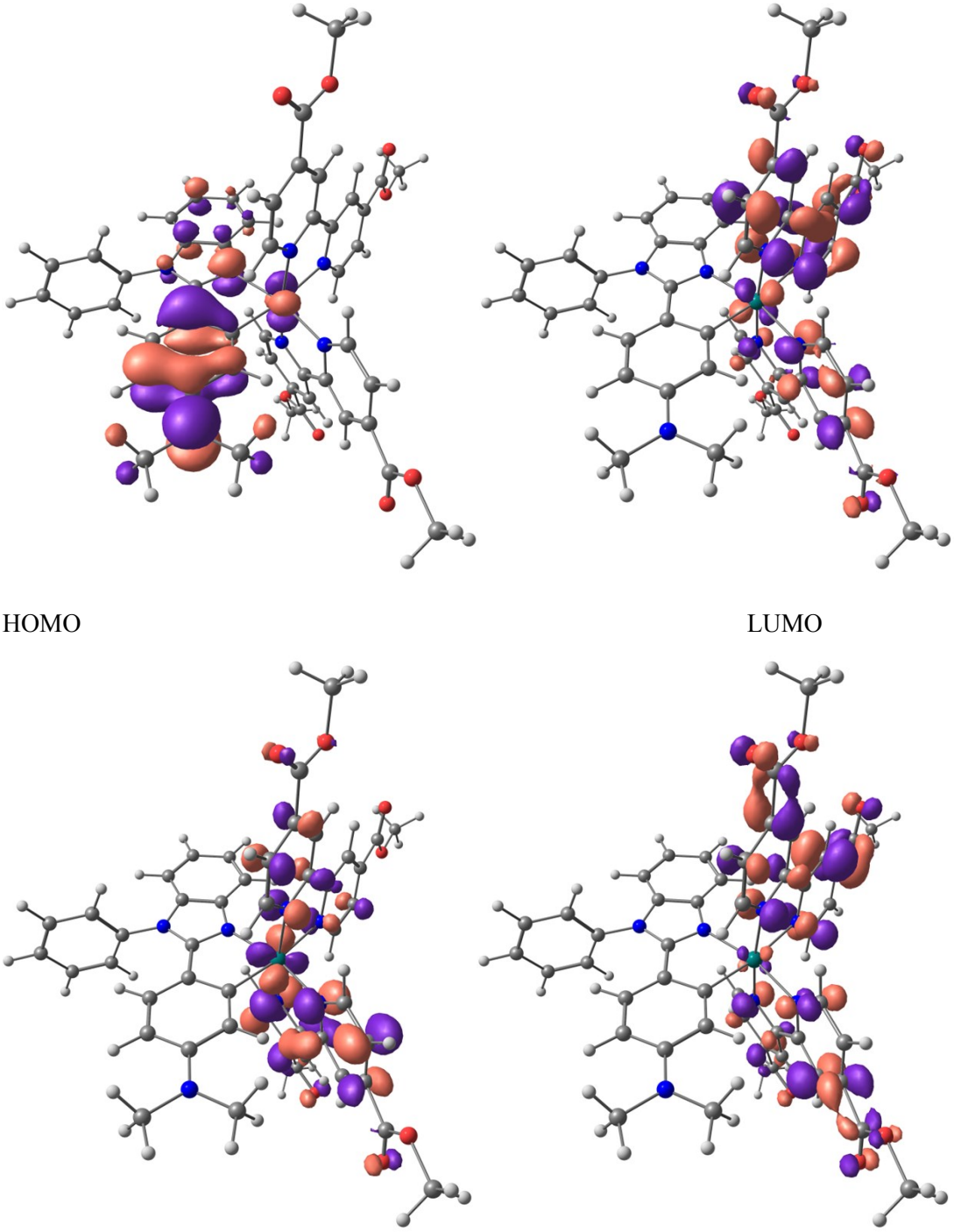

HOMO LUMO

LUMO+1 LUMO+2

Figure S38. Frontier molecular orbitals (HOMO-4 – LUMO+2) of complexes **1** – **5**.

6. Photovoltaic measurements.

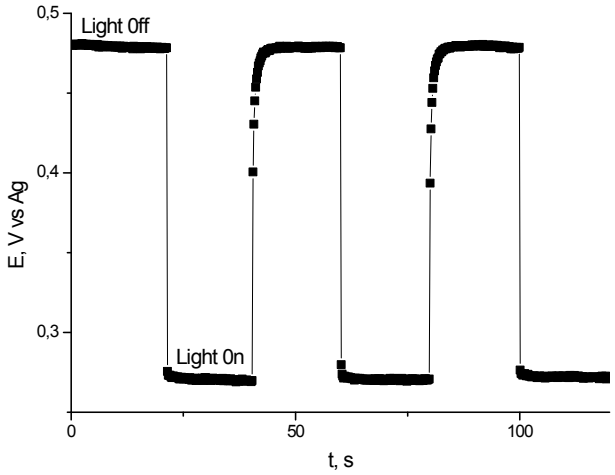

Figure S39**.** Time dependence of potential of TiO_2 photoanode sensitized by complex **1** in the dark and on exposure to AM 1.5 G simulated solar light (100 mW cm^{-2}) in acetonitrile solution in the presence of 0.5 M LiI + 0.05 M I_2

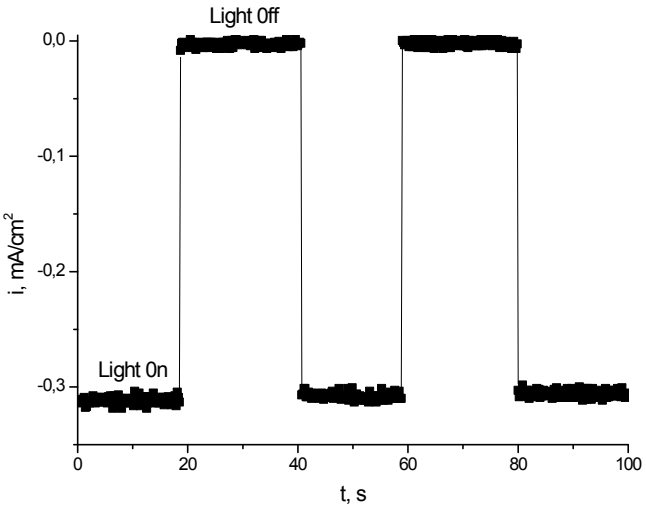

Figure S40**.** Time dependence of current at short circuit for PECC with TiO_2 photoanode sensitized by complex **1** in the dark and on exposure to AM 1.5 G simulated solar light (100 mW cm^{-2}) in acetonitrile solution in the presence of 0.5 M LiI + 0.05 M I_2

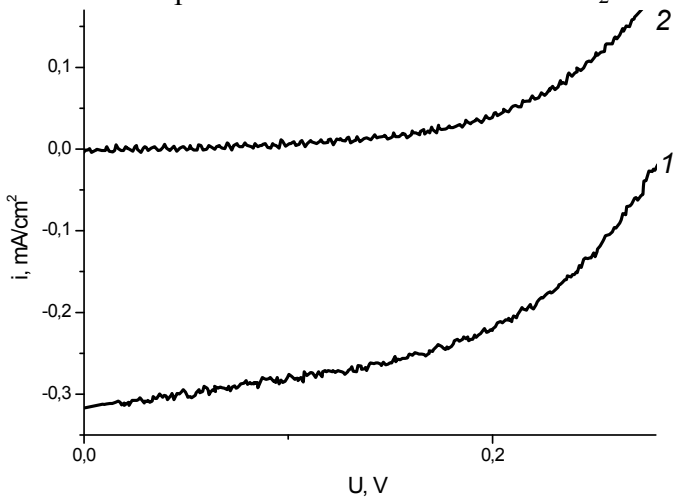

Figure S41. Current–voltage characteristic of a TiO_2 photoanode sensitized by complex **1** under AM 1.5 G simulated solar light (100 mW cm^{-2}) (1) and in the dark (2) in acetonitrile solution of 0.5 M LiI + 0.05 M I_2.

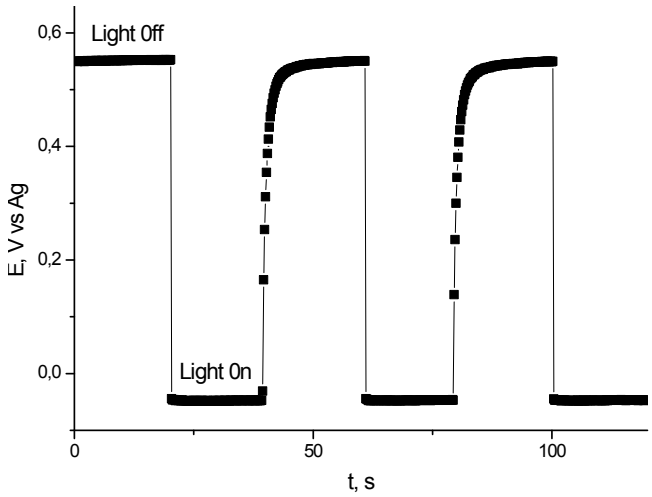

Figure S42**.** Time dependence of potential of TiO_2 photoanode sensitized by complex **2** in the dark and on exposure to AM 1.5 G simulated solar light (100 mW cm^{-2}) in acetonitrile solution in the presence of 0.5 M LiI + 0.05 M I_2

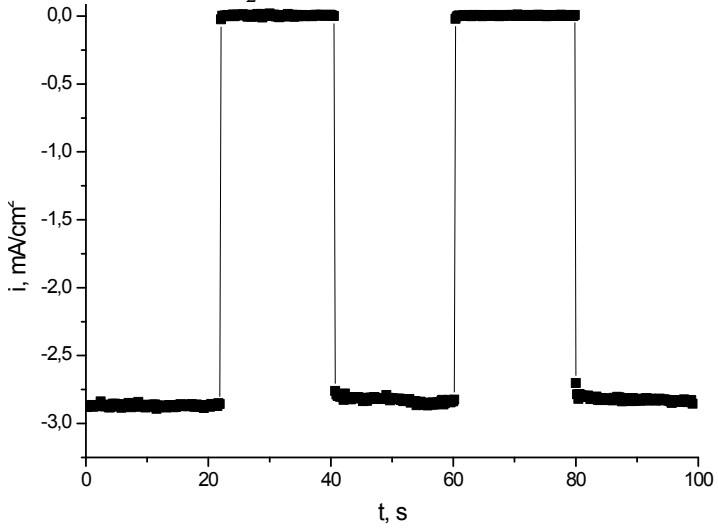

Figure S43**.** Time dependence of current at short circuit for PECC with TiO_2 photoanode sensitized by complex **2** in the dark and on exposure to AM 1.5 G simulated solar light (100 mW cm^{-2}) in acetonitrile solution in the presence of 0.5 M LiI + 0.05 M I_2

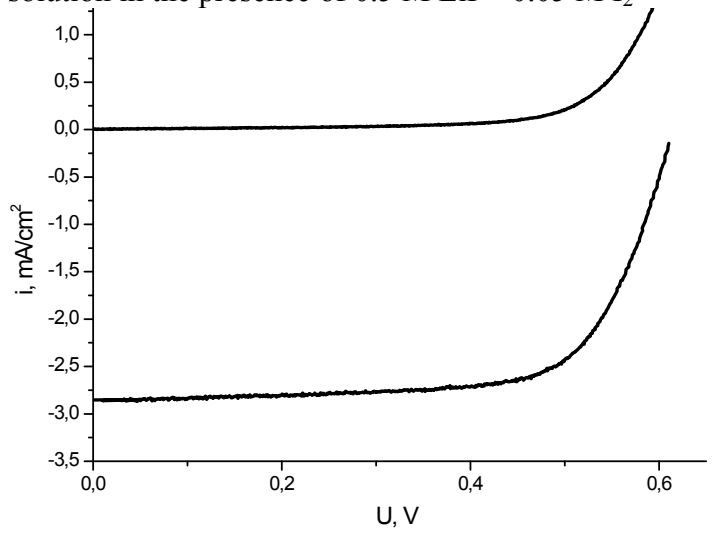

Figure S44. Current–voltage characteristic of a TiO_2 photoanode sensitized by complex **2** under AM 1.5 G simulated solar light (100 mW cm^{-2}) (1) and in the dark (2) in acetonitrile solution of 0.5 M LiI + 0.05 M I_2.

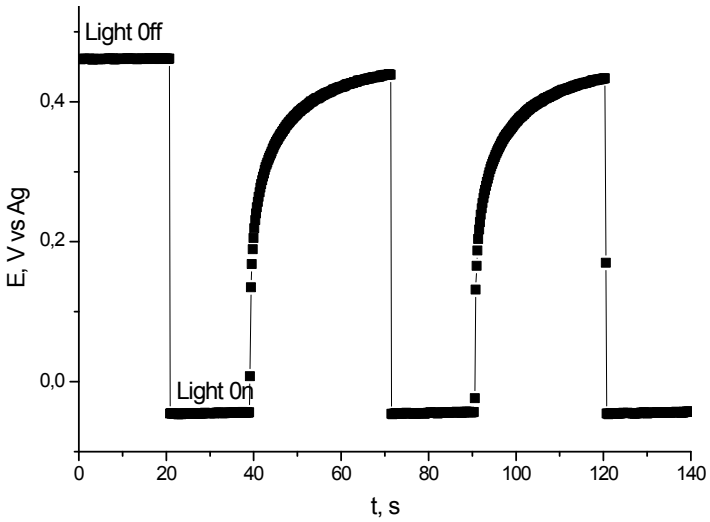

Figure S45**.** Time dependence of potential of TiO_2 photoanode sensitized by complex **3** in the dark and on exposure to AM 1.5 G simulated solar light (100 mW cm^{-2}) in acetonitrile solution in the presence of 0.5 M LiI + 0.05 M I_2

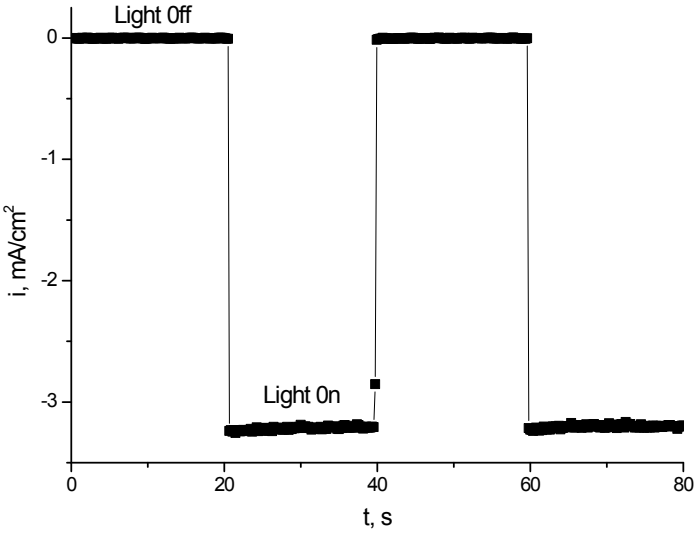

Figure S46**.** Time dependence of current at short circuit for PECC with TiO_2 photoanode sensitized by complex **3** in the dark and on exposure to AM 1.5 G simulated solar light (100 mW cm^{-2}) in acetonitrile solution in the presence of 0.5 M LiI + 0.05 M I_2

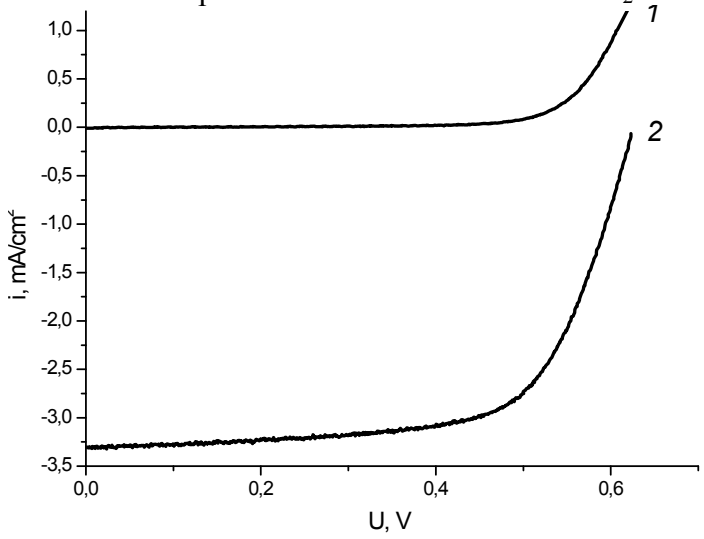

Figure S47. Current–voltage characteristic of a TiO_2 photoanode sensitized by complex **3** under AM 1.5 G simulated solar light (100 mW cm^{-2}) (1) and in the dark (2) in acetonitrile solution of 0.5 M LiI + 0.05 M I_2.

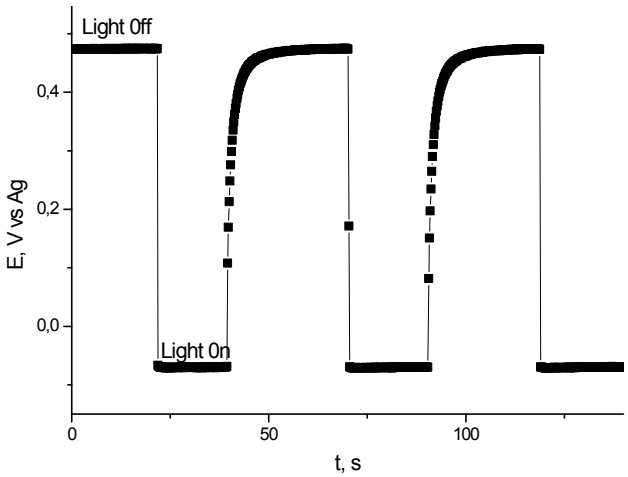

Figure S48**.** Time dependence of potential of TiO_2 photoanode sensitized by complex **4** in the dark and on exposure to AM 1.5 G simulated solar light (100 mW cm^{-2}) in acetonitrile solution in the presence of 0.5 M LiI + 0.05 M I_2

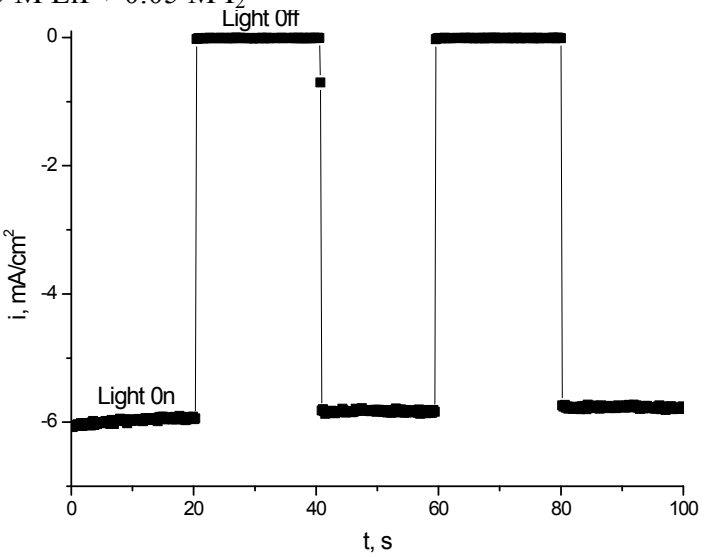

Figure S49**.** Time dependence of current at short circuit for PECC with TiO_2 photoanode sensitized by complex **4** in the dark and on exposure to AM 1.5 G simulated solar light (100 mW cm^{-2}) in acetonitrile solution in the presence of 0.5 M LiI + 0.05 M I_2

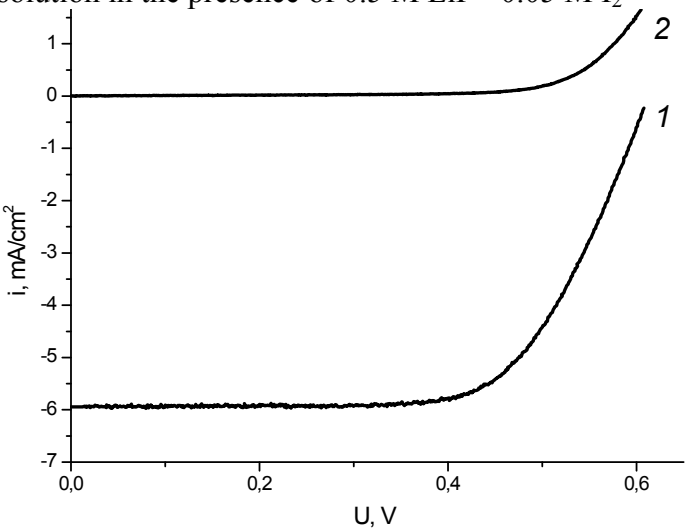

Figure S50. Current–voltage characteristic of a TiO_2 photoanode sensitized by complex **4** under AM 1.5 G simulated solar light (100 mW cm^{-2}) (1) and in the dark (2) in acetonitrile solution of 0.5 M LiI + 0.05 M I_2.

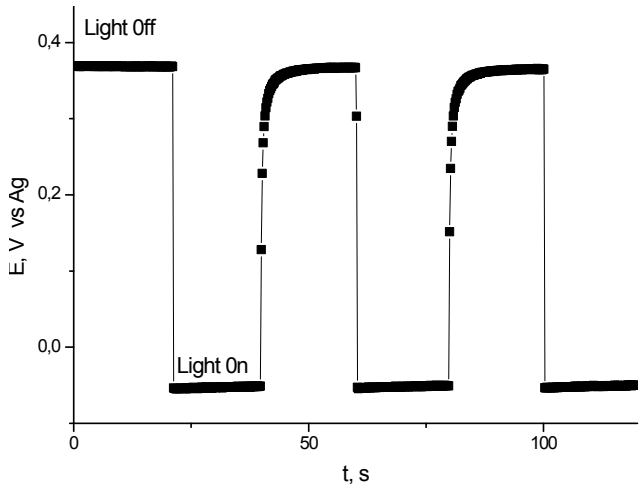

Figure S51**.** Time dependence of potential of TiO_2 photoanode sensitized by complex **5** in the dark and on exposure to AM 1.5 G simulated solar light (100 mW cm^{-2}) in acetonitrile solution in the presence of 0.5 M LiI + 0.05 M I_2

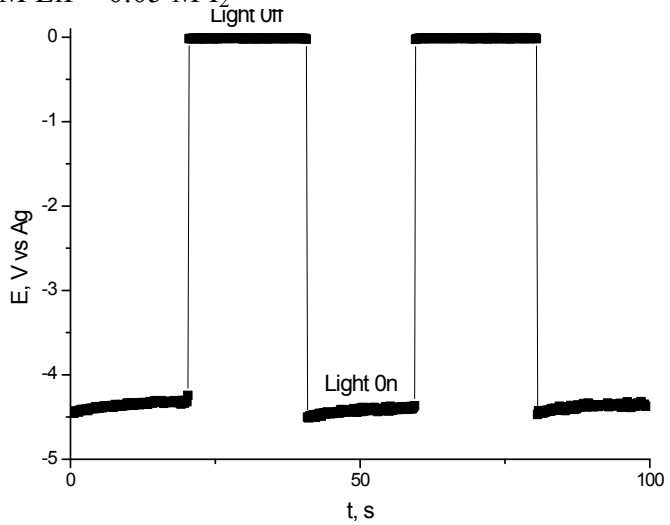

Figure S52**.** Time dependence of current at short circuit for PECC with TiO_2 photoanode sensitized by complex **5** in the dark and on exposure to AM 1.5 G simulated solar light (100 mW cm^{-2}) in acetonitrile solution in the presence of 0.5 M LiI + 0.05 M I_2

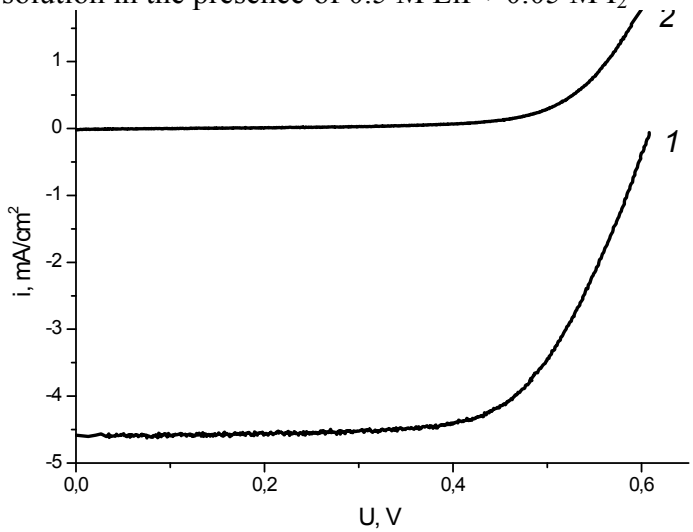

Figure S53. Current–voltage characteristic of a TiO_2 photoanode sensitized by complex **5** under AM 1.5 G simulated solar light (100 mW cm^{-2}) (1) and in the dark (2) in acetonitrile solution of 0.5 M LiI + 0.05 M I_2.